Applied Thermal Engineering 238 (2024) 121933

Contents lists available at ScienceDirect

Applied Thermal Engineering

journal homepage: www.elsevier.com/locate/apthermeng

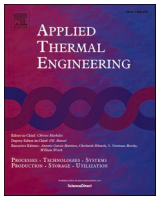

Research Paper

Experimental analysis of the effect of hydrogen as the main fuel on the performance and emissions of a modified compression ignition engine with water injection and compression ratio reduction

J.M. Rueda-Vázquez [a], J. Serrano [b,*], F.J. Jiménez-Espadafor [b], M.P. Dorado [a]

[a] Department of Physical Chemistry and Applied Thermodynamics, Córdoba University, Spain, Campus de Rabanales, Campus de Excelencia Internacional Agroalimentario ceiA3, 14071 Córdoba, Spain
[b] Department of Energy Engineering, Seville University, Spain, Camino de los Descubrimientos, s/n, 41092 Sevilla, Spain

ARTICLE INFO

Keywords:
Renewable fuel
CO_2 reduction
NO_x emissions reduction
High efficiency ICE

ABSTRACT

This study aimed to investigate the combined effects of compression ratio (CR), start of injection angle (SOI) and water injection (WI) on the performance, including NOx emissions, of a modified turbocharged compression ignition engine using H_2 as the primary fuel and diesel solely as a pilot ignition source. WI and H_2 were both injected into the intake manifold just after the charge heat exchanger. Test conditions varied the engine speed from 1500 rpm to 2750 rpm, covering a wide range of the original engine's operating conditions, water mass flow varied from 0 to 0.795 g/cycle and SOI for pilot ignition was studied in the range 10°, 5°, 0° before top dead center. Subsequently, the study examined the combined effect of reducing the engine's CR from 17.5:1 (base) to 13.5:1, in one-point increments, reducing SOI and water addition to further enhance the hydrogen energy share (HES).

HES varied from 0 % to 85 % under different engine conditions, and WI and SOI were employed to prevent knocking and ensure that the maximum combustion pressure did not exceed 160 bar. The test results indicate that NOx emissions increase with HES, but reducing the CR results in a reduction in NOx emissions of approximately 50 %. Additionally, WI further reduces NOx emissions by up to 50 %. The experimental evidence demonstrates that combining WI with CR and SOI reduction can effectively lower NOx emissions, achieving an efficiency greater than 35 % and therefore approaching the base diesel mode's efficiency. This also reduces the maximum in-cylinder pressure, allowing for an increase in turbocharger pressure and consequently enhancing the engine's specific power. The maximum engine power achieved was 31.6 kW at 2500 rpm (mean effective pressure of 10.1 bar), with a CR of 15.5, SOI at 10°, 1.5 kg/kWh of water, a HES of 81 %, and a minimum NOx level of approximately 480 ppm, with a maximum combustion pressure below 120 bar.

1. Introduction

To encourage the adoption of alternatives to fossil fuels and reduce greenhouse gas (GHG) emissions from hydrocarbon-based fuels in internal combustion engines in maritime and road transport, as well as electricity generation, governments have implemented stringent emission regulations [1,2].

Regarding road transport, the European Commission (EC) has proposed a 30 % reduction in CO_2 emissions limits for vehicles compared to the 2021 target, which was set at 95 g of CO_2 per kilometer [3]. Additionally, EC law now dictates that only power plants emitting less than 100 g of CO_2/kWh can be considered 'environmentally sustainable' [4,5]. These emission thresholds align with the Paris Agreement and are in line with the EU's scientific objective to achieve carbon neutrality by 2050.

In this regard, extensive efforts are being made to search for alternative fuels for diesel engines, such as oxygenated fuels like alcohol fuels, dimethyl ether, biodiesel fuels, and hydrogen as the most promising options. Biodiesel is a viable solution for diesel engines due to its biodegradable, oxygenated, sulfur-free, and renewable characteristics [6]. Blending biodiesel with fossil diesel offers several benefits, including reduced emissions, decreased engine wear, and comparable thermal efficiency compared to pure diesel fuel [7]. It's worth mentioning blends like diesel-tung oil-ethanol [8] and diesel-palm oil-ethanol [9]. In both cases, the feasibility of these blends as diesel fuel

* Corresponding author.
E-mail address: jserrano9@us.es (J. Serrano).

https://doi.org/10.1016/j.applthermaleng.2023.121933
Received 5 August 2023; Received in revised form 9 October 2023; Accepted 6 November 2023
Available online 7 November 2023

Nomenclature

ATDC	After top dead centre
BTDC	Before top dead centre
CFD	Computational Fluid Dynamics
CI	Compression ignition engine
CO	Carbon monoxide
CO_2	Carbon dioxide
C_p	Specific heat at constant pressure
CR	Compression ratio
DWI	Direct water injection
EC	European Commission
ECU	Electronic control unit
EGR	Exhaust gas recirculation
FB	Flow-blurring
FSN	Filter smoke number
GHG	Greenhouse gases
H_2	Hydrogen
H_2O	Water
HES	Hydrogen energy share
HRR	Heat release rate
ICE	Internal combustion engine
MEP	Mean effective pressure
N_2	Nitrogen
NO	Nitric oxide
NO_2	Nitrogen dioxide
NOx	Nitrogen oxides
OH	Hydroxyl radical
PM	Particulate matter
RPM	Revolutions per minute
SI	Spark ignition
SM	Single mode
SML	Single mode with partial low rate
SOC	Start of combustion
SOI	Start of injection
T	Temperature
TDC	Top dead centre
TM	Two modes
WCO	Waste cooking oil
WI	Water injection into the intake manifold

Greek symbols

α	Ratio between thermal capacity of the engine charge and fuel, both in terms of power
η	Efficiency
Δ	Delta increment

alternatives has been demonstrated using current diesel technology. Furthermore, extensive experimental work has been carried out to analyze the suitability of waste cooking oil (WCO) [10], where Joonsik Hwang and colleagues compared the performance of this fuel, highlighting a reduction in soot and CO emissions and a slight increase in indicated specific fuel consumption.

However, biodiesel has significant limitations as a complete alternative to petroleum derivatives due to several factors, such as elevated production costs, feedstock limitations related to competition with food production, the potential for deforestation, environmental concerns, and relevant regulatory and policy issues.

Therefore, the quest for sustainable and environmentally friendly energy solutions has sparked renewed interest in hydrogen as a clean alternative to conventional fossil fuels. Among the various applications of hydrogen as an energy carrier, internal combustion engines (ICEs) show significant promise due to their adaptability to existing infrastructure and their potential to facilitate the transition to a hydrogen-based economy.

When coupled with innovative technologies that offer flexibility to meet the engine's required characteristics [11,12], H_2 offers several advantages:

1. Zero carbon content (despite not existing freely in nature, hydrogen is the most abundant element in the universe) [13].
2. It can be produced from renewable energy sources, although currently, 95 % of hydrogen is generated using methods based on fossil fuels [14].
3. It possesses a very high energy density of 120 MJ/kg, which is around 3 times that of hydrocarbon-based fuel.
4. Extensive research is currently underway for both hydrogen production and storage [12,13].

However, it is worth noting that when it comes to hydrogen storage, there are some drawbacks, such as its low volumetric energy density, which necessitates large storage areas and makes it expensive. Compressed H_2 storage is the most established hydrogen storage technology and involves pressurizing H_2 in high-pressure vessels; with the current technology based on wrapped composite cylinders, pressures of up to 1000 bar can be achieved [15]. However, there are new exploration areas, such as electrochemical hydrogen storage materials in nanostructures [16,17]. In these cases, researchers are seeking materials with a large surface area as well as proper porosity for H_2 storage [18,19], which appear to have significant potential.

Using H_2 as a fuel in an internal combustion engine (ICE) involves significantly different combustion properties compared to hydrocarbon-based fuels. Hydrogen burns much faster than these fuels, which means that achieving high efficiency with H_2 in an ICE requires optimizing the shape of the combustion chamber, adjusting the CR, and calibrating the ignition timing to prevent damaging knock [20], minimize elevated NOx emissions [21,22], reduce high in-cylinder peak pressures and temperatures, and improve engine performance [23].

On the other hand, the high diffusivity of hydrogen allows for a perfect mixture with air, achieving almost complete homogeneity when introduced into the combustion chamber. Although H_2 can be used in both spark ignition (SI) [24,25] and compression ignition engines (CI) [26], it cannot be directly used in CI engines due to its higher self-ignition temperature (850 K). This would require an impractically high CR or heating the intake air, which ultimately reduces volumetric efficiency and engine power. However, H_2 can be utilized in CI engines in dual-fuel mode by using diesel fuel as an ignition source. Typically, gaseous H_2 fuel is supplied to the intake manifold, and diesel fuel is directly injected into the combustion chamber as the ignition source. However, this approach results in reduced volumetric efficiency since H_2 displaces part of the intake air during the intake stroke [27].

There are two drawbacks related to using H_2 as fuel in CI engines: NOx generation and knocking, which prevent achieving maximum power. In this regard, there are several strategies for controlling them, such as exhaust gas recirculation (EGR), direct water injection (DWI), or water injection into the intake manifold (WI) [28]. All of these strategies aim to reduce in-cylinder temperatures, primarily through the Zeldovich mechanism, which is one of the main mechanisms that contribute to NOx formation. The addition of water has various effects on combustion, including a decrease in in-cylinder temperature, resulting from the increased heat capacity of the mixture (thermal effect); a delay in the SOC due to reduced load temperature; a minor chemical effect on engine combustion due to OH radicals from water [29]; and a decrease in oxygen concentration (dilution effect), which leads to reduced NOx emissions.

Table 1
Summary of the primary experimental studies currently published on H_2 dual fuel CI engines with H_2.

Author (reference)	H_2 enrichment and mixing process	Engine specifications	WI/CR tested	Key findings
Works with both WI and CR reduction				
Chintala and Subramanian [34]	32 % HES (Manifold injection)	Single cylinder Max Power: 7.4 kW at 1500 rpm	WI 130–410 g/kWh CR 19.5:1 16.5:115.4:1	NOx emissions decrease with higher WI rates. (CR 19.5:1, 130 g/kWh WI) NOx = 9.7 g/kWh (CR 19.5:1, 270 g/kWh WI) NOx = 6.5 g/kWh (CR 19.5:1, 410 g/kWh WI) NOx = 5.1 g/kWh Max. in-cylinder temperature decrease with higher WI rates. (CR 19.5:1, 340 g/kWh WI) T = 1784 K (CR 16.5:1, 340 g/kWh WI) T = 1437 K (CR 15.4:1, 340 g/kWh WI) T = 1248 K
Raju and Masimalai [35]	8 % HES (Manifold injection)	(Numerical study) Single cylinder Max Power: 3.67 kW at 1500 rpm	WI 3–7 % by mass CR 16.5:115.5:1	Results predict a rise in in-cylinder temperature at 8 % HES, which also increases knocking and NOx emissions. The higher in-cylinder temperature as well as its effects are reduced by the use of WI and also by reducing the CR in parallel.
Works with WI				
Chintala and Subramanian [36]	0–39 % HES (Manifoldinjection)	Single cylinder Max Power: 7.4 kW at 1500 rpm	WI 0–270 g/kWh	NOx emissions increase with higher HES. NOx emissions are reduced a maximum of 37 % with 270 g/kWh WI, with the penalty of a slight increase in carbon-based emissions.
Chintala and Subramanian [37]	18 % HES (Manifoldinjection)	Single cylinder Max Power: 7.4 kW at 1500 rpm	WI 200 g/kWh	NOx emissions increase with higher HES. (No H_2, No WI) NOx = 6.9 g/kWh (19 % HES, No WI) NOx = 9.7 g/kWh (19 % HES, 200 g/kWh WI) NOx = 6.6 g/kWh
Serrano et al [29]	0–74 % HES (Manifold injection)	Four cylinders Max. Power: 63 kW at 4000 rpm	WI 0–48 kg/h	NOx emissions increase with higher HES. NOx emissions decrease with higher WI rates. WI from 0 to 16 kg/h produces a reduction in NOx emissions of approximately 70 %, compared to the cases without WI.The thermal mechanism clearly dominates and provides a minimum value for NOx emission with regard to the thermal capacity of the engine load.
Works with CR reduction				
Chintala and Subramanian [22]	0–63 % HES (Manifold injection)	Single cylinder Max Power: 7.4 kW at 1500 rpm	CR 19.5:1 16.5:115.4:1	NOx emissions decrease with lower CRs. NOx emissions increase with higher HES. (CR 19.5:1, 19 % HES) NOx = 9.7 g/kWh (CR 16.5:1, 19 % HES) NOx = 5.5 g/kWh (CR 15.4:1, 19 % HES) NOx = 5 g/kWh
Masood et al [30]	8.3–30.1 % HES (Direct Injection)	Single cylinder Max. Power: 3.7 kW at 1500 rpm	CR 24.5:1 22:1 20:1 18.35:116.35:1	NOx emissions decrease with lower CRs. NOx emissions increase with higher HES. (CR 24.5:1, 90 % HES) NOx = 38 % higher than 10 % HES. (CR 18.35:1, 90 % HES) NOx = 27 % higher than 10 % HES. (CR 24.5:1, 90 % HES) NOx = 38 % higher than CR 16.35:1.
Rosha et al [38]	0.5 kg/h (H_2-enriched biogas) (Manifold Injection)	Single cylinder Max. Power: 3.5 kW at 1500 rpm	CR 18:1 17:116:1	NOx emissions decrease with lower CRs. (CR 18:1, 3.5 bar MEP) NOx = 16.5 g/kWh (CR 17:1, 3.5 bar MEP) NOx = 13.2 g/kWh (CR 16:1, 3.5 bar MEP) NOx = 12.6 g/kWh
Yilmaz [39]	0–37.6 % HES (Manifold Injection)	Four cylinders Max Power: 48 kW (4000 rpm)	CR 18.25:116.9:1	H_2 enrichment and low CR can be used to reduce the maximum in-cylinder pressure and HRR and prevent abnormal combustion without deteriorating the BTE.

Another alternative for controlling NOx emissions and knocking and addressing the challenges associated with using H_2 as a fuel, is the reduction of the CR in CI engines. Masood et al. [30] analysed CR reduction in dual-fuel engines (H_2-diesel) and reported an increase in the amount of H_2 that can be used. However, the efficiency of the engine in dual-fuel mode decreases with CR reduction due to reduced combustion efficiency and lower in-cylinder temperatures resulting from the lower CR [31,32]. Another focus is provided by V. Chintala et al. [22], where CR reduction and WI operated in a CI under dual-fuel mode allowed a significant reduction in NOx emissions compared to the base diesel mode but slightly higher than the conventional dual-fuel mode. A notable conclusion emerging from this study is that the combined strategy of water addition and CR reduction is a promising solution for a drastic enhancement of the maximum hydrogen energy share.

This paper presents the results of an experimental investigation into the combustion characteristics and NOx emissions of a hydrogen-fueled internal combustion engine equipped with a water injection system. The study focuses on exploring the influence of hydrogen concentration, water injection volume, and CR on MEP, NOx emissions, ignition delay, maximum in-cylinder pressure, and efficiency under various engine loads and speeds. The combination of hydrogen as the primary fuel and water injection as a control strategy has the potential to enhance combustion stability, mitigate knock risk, decrease peak temperatures, and reduce NOx formation during the combustion process. The analysis carried out in this work regarding the combined effects of CR, SOI, WI, and HES on combustion and performance at four different RPM settings in a four-cylinder turbocharged diesel engine has not been undertaken by other researchers. This is evident from the review by Pali Rosha et al. [33] and the research conducted by V. Chintala [34], enabling the projection of the study's results to a practical implementation.

To gain a comprehensive understanding of the current state of technology regarding the use of H_2 as fuel in CI engines and facilitate a comparison with the analysis conducted in this work, Table 1 presents a summary of the primary experimental studies currently published. As can be seen in Table 1 and as will be discussed later, this work covers a broader range of parameters:

- The minimum CR studied in this work is 13.5:1, while other researchers have either focused on a single CR or studied down to 15.4:1. [22,30,34,35,38,39].

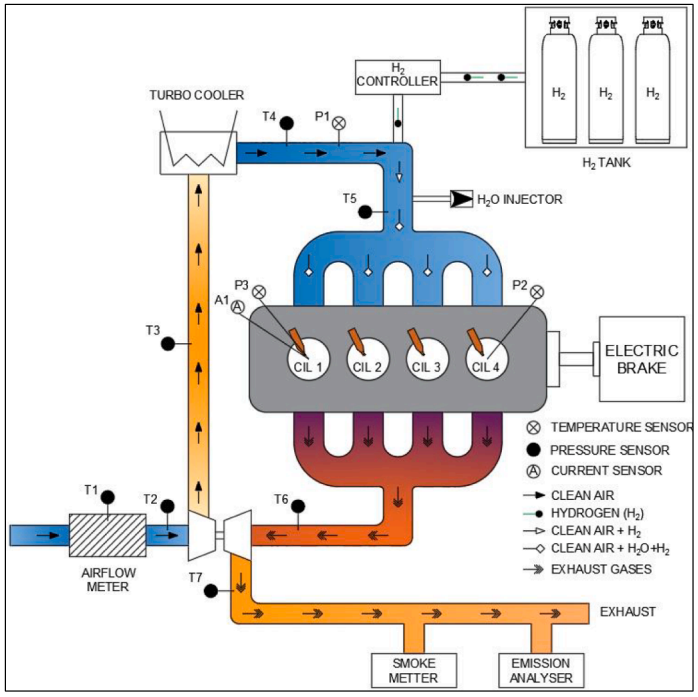

(a)

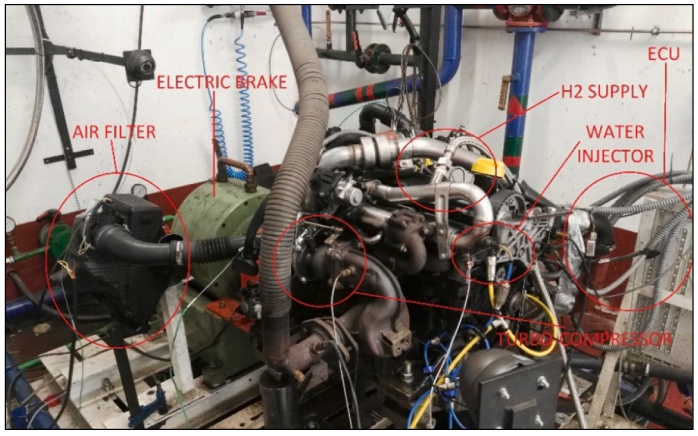

(b)

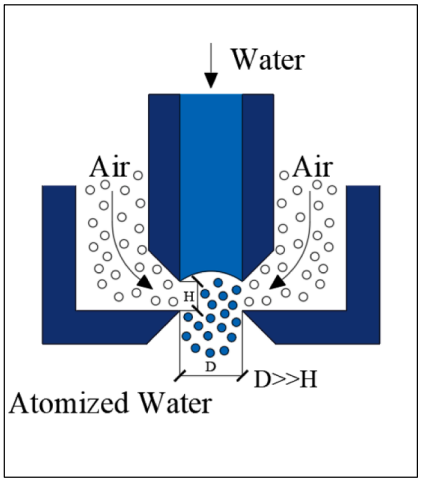

(c)

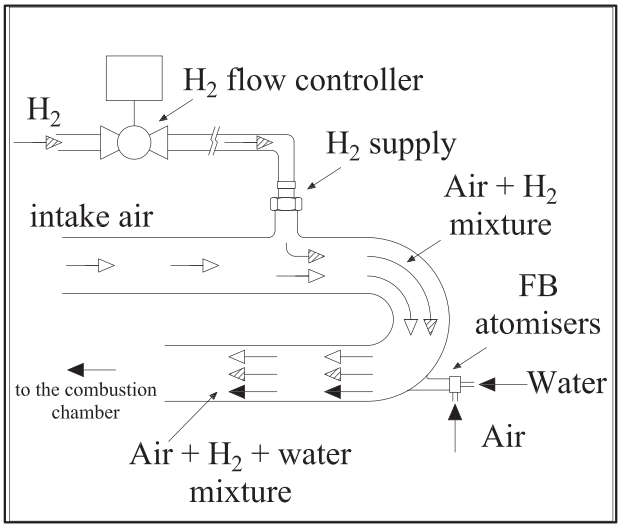

(d)

Fig. 1. (a) Schematic diagram of the experimental setup. (b) Photograph of the experimental test rig. (c) Schematic diagram of the FB atomizers. (d) Schematic diagram of the H_2 supply and water addition system.

Table 2
1.5dCi k9k 766 Engine characteristics in diesel-only mode.

Type	*4 S, 4 cylinders*
Engine displacement	*1461 cm^3*
Bore	*76 mm*
Stroke	*80 mm*
Compression ratio	*17.5:1*
Maximum power	*63 kW at 4000 rpm*
Maximum torque	*220 Nm at 1800 rpm*
Fuel	*Diesel EN590*
Lubrication	*Gear oil pump*
Injection pump	*Distributor injection pump with common rail*
Injector	*Solenoid type*
EGR	*Valve controlled and water cooled*
Turbocharger	*Turbine controlled by waste gate valve*
Engine refrigeration	*Water cooled*
Charge air	*Water cooled*

- In this work, the range of HES has been continuous, spanning from 0 to 85 %, while previous studies have focused on specific values of HES or reduced ranges [22,30,29,34,35,36,37].
- The combination of WI and CR in a current technology engine, turbocharged and with 4 cylinders, has only been studied in this work; the rest of experimental analyses involving CR and WI have been conducted on naturally aspirated single-cylinder engines [29].
- The analysis performed in this work has covered a range from 1500 rpm to 2750 rpm, whereas results provided by other researchers have been reported at only one RPM [22,34,35,36,37,38,39].
- The maximum MEP achieved with H_2 (with diesel fuel only for ignition) is the same as that of the original diesel engine at maximum power. There is no published work where the performance has been analyzed at this MEP.

The objectives of this research are as follows:

1. To evaluate the influence of water injection on combustion characteristics and efficiency in a hydrogen-powered ICE at varying CR, while relying solely on diesel fuel for ignition, over a wide range of CR values.
2. To quantify the reduction in NOx emissions achieved by employing WI, varying SOI, and adjusting CR across a broad range of RPMs, all while maximizing HES.
3. To assess the trade-offs between performance and emissions control in a hydrogen-powered ICE by examining the effects of varying compression ratios, SOI timing, and WI strategies.

2. Experimental setup

The experimental analysis conducted in this study was performed on a commercial diesel engine that was modified to enable the measurement of combustion pressure, utilize hydrogen as a fuel source, and introduce water injection into the intake manifold (refer to Fig. 1). The original engine is the Renault model 1.5 dCi k9k 766, and its key characteristics are detailed in Table 2. In this research, we investigated five different compression ratios: 17.5:1, 16.3:1, 15.5:1, 14.5:1, and 13.5:1. These ratios were achieved by modifying the piston head shape. Commercial solutions exist for 17.5:1 and 15.5:1, as illustrated in Fig. 2 (a) and (c). However, for 16.3:1, 14.5:1, and 13.5:1, grooves of varying depths were created to remove material of from the piston head, demonstrated in Fig. 2(b), (d), and (e). Specifically, for 16.3:1, the grooves were incorporated into the 17.5:1 commercial piston, while for 14.5:1 and 13.5:1, they were implemented in the 15.5:1 commercial piston.

Table 3 lists all the sensors installed in the engine system depicted in Fig. 1. The temperature and pressure sensors are denoted by the letters "T" and "P," respectively, while the ammeter is represented by the letter "A." The P2 and P3 pressure sensors are "ThermoCOMP™ Quartz" water-cooled measuring probes designed with compact dimensions, particularly suitable for use in internal combustion engines with reduced volume and more than 2 valves per cylinder. The pressure sensor model is 6043A60 by Kistler [40]. The ammeter measures the current signal of the injector, enabling simultaneous measurement of the injection duration and the start of injection angle.

The engine configuration and timing were adjusted using the Commander 4DE from Sybelle, which is the electronic control unit (ECU) capable of modifying most of the engine parameters [41]. In the context of this study, this unit was utilized to manage the following engine subsystems: the start of injection angle (SOI), the quantity of fuel for pre-injections, and the achievable turbocharger pressure (via a map correlating RPM and injection quantity). Although the engine was equipped with an exhaust gas recirculation valve (EGR), it was deactivated for this research.

In this study, NOx exhaust gas emissions were measured using a Testo 350 XL. The opacity of the exhaust gas was assessed with an AVL Smoke Meter 415SE, which employed the filter paper method to determine the filter smoke number (FSN), as defined by ISO 10054.

3. Experimental tests

The engine running on hydrogen was studied examined at four different speeds (1500, 2000, 2500, and 2750 rpm) and various SOI settings (+10°, +5°, and 0° BTDC). For each SOI setting, the amount of diesel fuel injected was adjusted to achieve the target speed (without hydrogen) and ~~no~~ without any applied brake load. The engine's waste-gate control was deactivated, resulting in the intake pressure being set to the maximum attainable level based on the exhaust conditions at the turbine inlet.

The tests were conducted for each CR as follows: at each engine RPM and SOI combination, the mass flow of hydrogen was incrementally increased gradually raising engine torque and as observed, leading to higher NOx levels. When the NOx emissions reached a certain threshold or if knocking was detected, water was injected using FB atomizers (to minimize water coalescence), effectively reducing NOx levels but affecting the HRR and overall engine performance. The test continued until one of the following limits was reached, although both typically ~~met~~ occurred simultaneously:

- The maximum allowable in-cylinder pressure to ensure mechanical integrity is approximately 150–160 bar.
- Combustion knocking.

The annex shows the various tested conditions, with over 469 tests conducted, and provides the minimum and maximum values for the following variables: hydrogen mass flow, water mass flow, diesel mass flow, torque, power, MEP, efficiency, and the (diesel + H_2)/air ratio. A positive main injection angle indicates that the SOI occurs before TDC.

The test conditions allow for the investigation of the interaction between H_2 and water, as well as the efficiency and the fundamentals of NOx formation. Furthermore, these test conditions have enabled the attainment of a mean effective pressure of 11.3 bar, which represents 90 % of the mean effective pressure of the diesel engine at maximum power (12.6 bar). This allows for a meaningful comparison between the hydrogen-based solution and the diesel engine.

In this experimental study, in-cylinder temperature and HRR were determined using a 0-D thermodynamic model developed by J. Serrano et al., as cited in Ref. [29]. As outlined in Section 2, modifications were made to the piston heads to achieve the desired CR, resulting in changes in bowl shape and the cylinder/bowl ratio for each CR. While these modifications may influence mixture formation and diesel combustion, the minimal quantity of diesel injected and its correspondingly short duration ensure that the combustion chamber's shape does not significantly impact diesel combustion or the SOC, as illustrated below.

Figs. 3 and 4 depict the injection pulse intensity in amperes, as

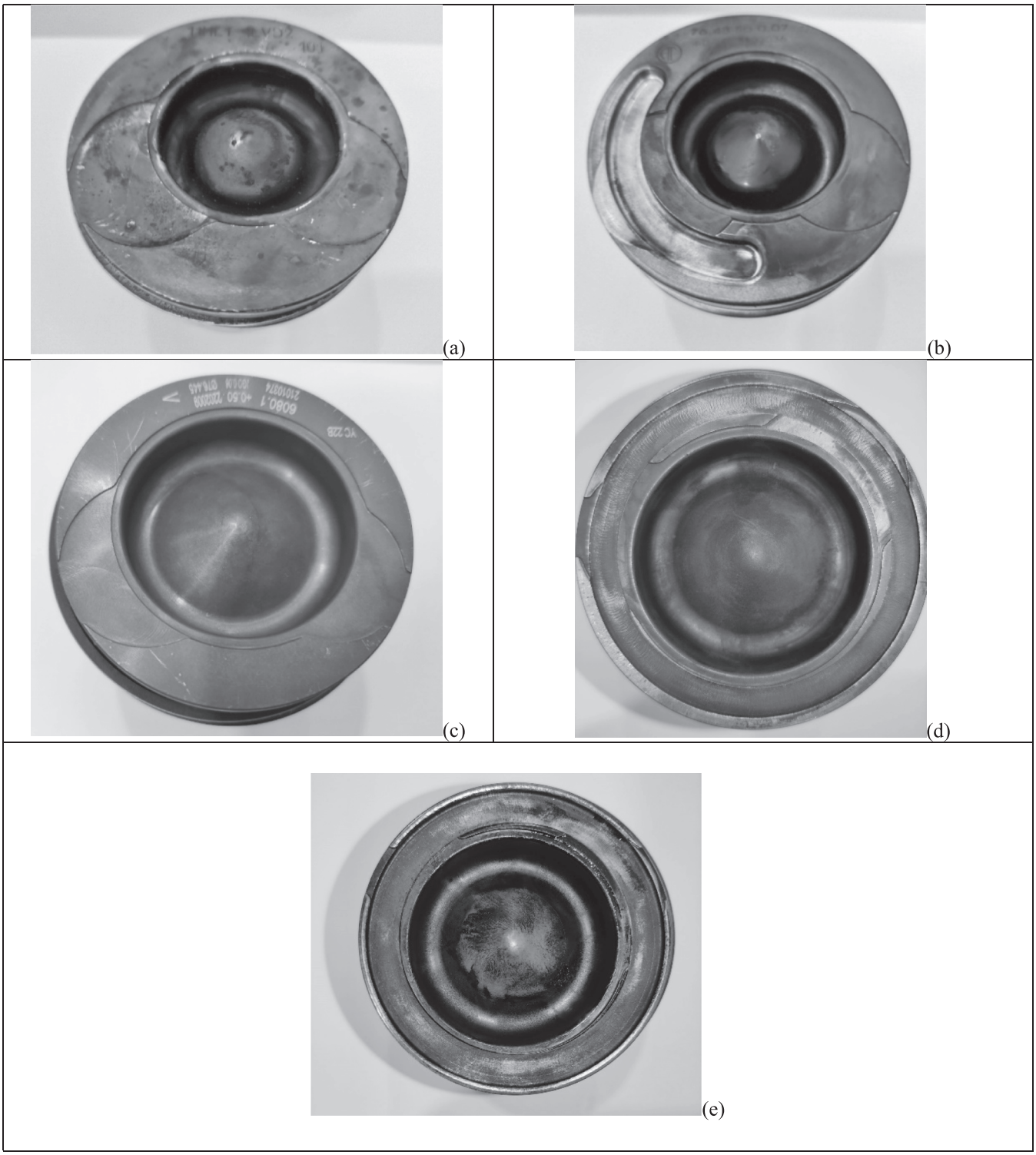

Fig. 2. Photographs of the different combustion chamber. (a) CR = 17.5, (b) CR = 16.3, (c) CR = 15.5, (d) CR = 14.5 and (e) CR = 13.5.

measured by the ammeter in Fig. 1a, along with the combustion pressure and the HRR curve, which enables the assessment of the SOC. It is evident that, in all conditions, the SOC occurs after the conclusion of injection. As a result, all of the diesel fuel is inside the combustion chamber before the combustion process initiates, ensuring an ample supply of air for the fuel–air mixture. Under these circumstances, the SOC is solely dependent on the pressure–temperature history of the fuel [42] since the SOI, with no significant influence from the combustion chamber shape. The opposite scenario would be applicable to typical diffusive combustion when the entire range of engine power is solely provided by diesel.

The smallest difference between the end of injection and the SOC occurs at the highest CR, mainly due to the higher charge temperature associated with this CR. It is also noticeable at the highest engine speed, primarily because of the increased quantity of diesel injection, particularly when water injection is not utilized. This is illustrated in Fig. 4(a), where, under these conditions, the injection concludes just before the SOC, as confirmed by the comparison between the injection pulse and

Table 3
Sensors used in the experimental apparatus.

Temperature sensors			
Position	Comments	Unit	Measurement accuracy
T1	Mass air flow	°C	(-40 + 120) °C (≤3 %)
T2	Intake air before compressor		0–1000 °C ± 1.5 °C
T3	Intake air after compressor		
T4	Intake air after cooler		
T5	Intake air after water injection		
T6	Exhaust flow before turbine		
T7	Exhaust flow after turbine		
Pressure sensors			
Position	Comments	Unit	Measurement accuracy
P1	Outlet compressor pressure	bar (absolute)	0–10 bar (≤0.5 %)
P2	Combustion pressure inside	bar (relative)	0–250 bar ± 0.5 %
P3	cylinder		
Current sensor			
Position	Comments	Unit	Measurement accuracy
A1	Ammeter	A	0–30 A ± 1 %

the HRR.

WI also results in a delay in the SOC, as demonstrated in Fig. 3(b) and Fig. 4(b) (this aspect will be further discussed in Section 4.3). In these figures, a positive crank angle value indicates "after Top Dead Center" (ATDC), while a negative value indicates "before Top Dead Center" (BTDC). When comparing the injection duration between the lowest engine running speed (Fig. 3) and the highest engine speed (Fig. 4), it becomes evident that the injection pulse lasts longer (in terms of crank angle) in the latter case due to the increased pilot fuel quantity at higher engine speeds, as specified in the annex. This extended duration is necessary to counteract the rising friction losses associated with higher engine speeds.

4. Results and discussion - performance and emissions with different compression ratios

The analysis of the experiments focuses on four specific aspects: NOx emissions, engine efficiency, SOC analysis, and maximum combustion pressure. In hydrogen-based fuel engines, increasing the hydrogen energy share (HES) also results in an increase in NOx emissions due to faster combustion resulting from the high diffusivity and flame speed of hydrogen. To mitigate this undesirable effect, various strategies can be employed: modifying the SOI, enabling exhaust gas recirculation (EGR, which is not studied in this work), implementing WI, and reducing the CR. These strategies could offer solutions to enhance the maximum HES, leading to increased engine specific power, reduced NOx emissions, improved engine efficiency, and, for these reasons, the effects of CR, SOI angle, and WI will be studied in this section through the analysis of MEP, efficiency, SOC, HRR, and in-cylinder maximum pressure.

The HES is evaluated using the dimensionless Equation (1), and in the experiments conducted in the annex, it falls within the range of 48 % to 85 %:

$$HES = \frac{m_{H_2} \bullet LHV_{H_2}}{m_{H_2} \bullet LHV_{H_2} + m_{diesel} \bullet LHV_{diesel}} \quad (1)$$

All the figures presented in this paper follow the same legend structure. Each colour and symbol represent varying values for H_2O mass flow, measured in grams per cycle, and different levels of HES.

Regarding SOC, this can be seen as a contributing factor in explaining the effects of H_2 and WI. Although SOI is the independent variable, SOC is the one that is truly important for understanding the impact of SOI on emissions and efficiency. Furthermore, SOC is sensitive to CR, HES, and WI because it exhibits a high dependency on charge temperature.

Hydrogen combustion generates only water and does not produce any PM (soot). Soot originates from the diesel fuel used for ignition in the combustion process and consistently remains at low levels in all tests, below 2 mg/m^3. For this reason, it has not been included in the analysis.

4.1. No_x emissions analysis

The formation of NOx is primarily explained by the Zeldovich mechanism, which exhibits a strong dependence on temperature and a lesser dependence on the fuel–air equivalence ratio. NOx is generated through the oxidation of N_2 present in the inducted air, driven by the high in-cylinder temperature, and is primarily composed of NO with smaller amounts of NO_2. The rapid combustion of H_2 tends to elevate the gas temperature ~~on~~ in the combustion chamber, thereby promoting the formation of NOx. In this study, under identical operational conditions (RPM, SOI, HES, and H_2O mass flow), it is observed, ~~at~~ as expected, that NOx emissions decrease as the CR decreases.

Figs. 5 and 6 illustrate the evolution of NOx emissions versus CR at different SOI and RPM, while considering HES and WI as parameters. Meanwhile, Fig. 7 depicts the calculated mean combustion temperature of the gases within the combustion chamber versus crank angle, considering different HES, RPM, and SOI, and utilizing CR and WI as parameters.

The dependence of NOx on RPM is clearly evident for all the tested conditions and the five different CR values. When examining Fig. 5(a), (b), and (c), all of which have the same SOI of 10°, the maximum NOx concentration decreases progressively from approximately 1000 ppm at 2000 rpm to below 600 ppm at 2750 rpm. In the case of a 5° SOI, as seen in Fig. 6(a) and (b), NOx decreases from a peak of 800 ppm at 1500 rpm to 300 ppm at 2750 rpm, with nearly the same HES. This trend across RPM, which applies to all conditions, is attributed to the kinetics of NOx formation. Considering that the combustion process occurs within a crank angle range of 5° to 25°, as engine RPM increases, the available time for complete NOx formation diminishes, resulting in less time for NOx to fully develop. Therefore, from this perspective, the higher the RPM, the lower the expected NOx formation.

The dependence of NOx on SOI can be observed across the tested conditions and the five different CR values. When comparing Fig. 5(a), 6 (a), and (c), where the SOI is 10°, 5°, and 0° respectively, the maximum NOx concentration progressively decreases from approximately 1000 ppm at SOI 10° to roughly 300 ppm at SOI 0°. Additionally, examining Fig. 5(c) and 6(b), both at 2750 rpm and with a SOI of 10° and 5°, respectively, NOx decreases from 600 ppm to 300 ppm. This behaviour is attributed to the significant dependence of NOx formation on temperature. Once combustion begins, NOx forms at the flame front (which is very narrow due to the high pressure inside the combustion chamber), but as pressure and temperature continue to increase, NOx continues to form in the burned area. When SOI is reduced, there is also a reduction in SOC (achieve negative values), as can be seen when comparing Fig. 7 (a) and (b). Consequently, the portion of combustion occurring at higher pressure and temperature decreases, leading to a reduction in NOx generation. This effect is clearly evident when examining Fig. 7(a) and (b), both at 2000 rpm, with SOIs of 10° and 0°, respectively. The consistent temperature reduction with decreasing SOI aligns with the previously mentioned trend. In particular, it can be observed that at CR 17.5 and with approximately the same HES, the maximum temperature decreases by 200 °C. With a reduced CR, the loss in maximum temperature is around 100 °C.

The dependence of NOx on HES can be observed when we exclude the effects of WI; therefore, only the cases with 0 g/cycle of water are considered here. When examining Fig. 5(a) (2000 rpm and SOI 10°) and comparing HES levels of 45 % and 62 %, NOx increases from 420 to 900

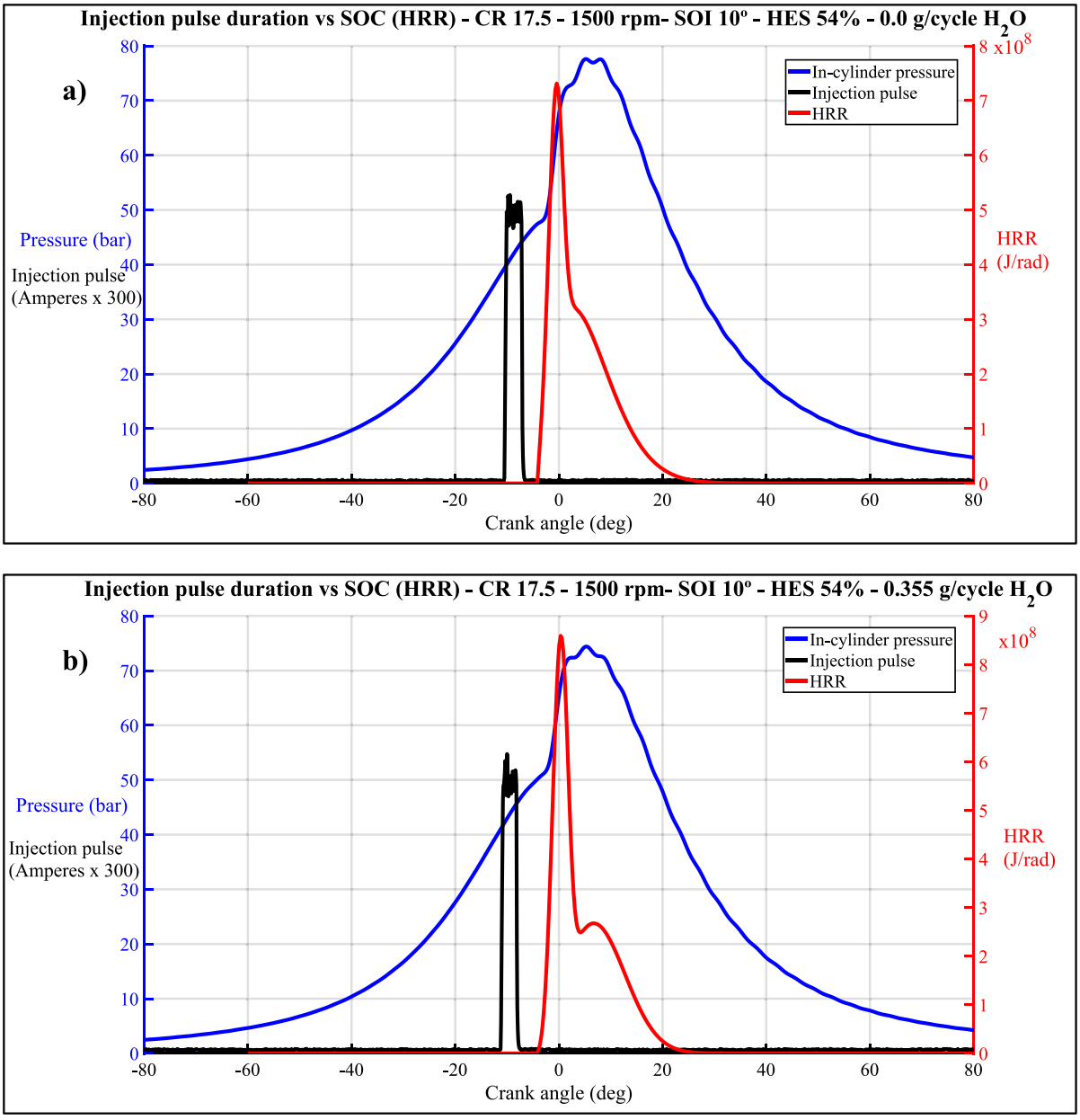

Fig. 3. (a) Comparison of the injection pulse duration and the SOC through the HRR at 1500 rpm and SOI 10° for CR 17.5, HES 54 % and 0.0 g/cycle H_2O. (b) Comparison of the injection pulse duration and the SOC through the HRR at 1500 rpm and SOI 10° for CR 17.5, HES 54 % and 0.355 g/cycle H_2O.

ppm, respectively. In Fig. 5(b) (2500 rpm and SOI 10°), NOx emissions continuously rise from 340 ppm at 38 % HES to 810 ppm at 64 % HES in an almost quadratic fashion. In Fig. 5(c) at 2750 rpm (the highest tested) and SOI 10°, NOx emissions increase from 240 ppm at 34 % HES to 590 ppm at 61 % HES. This continuous increase in NOx with HES is attributed to the rise in combustion gas temperature resulting from the increased presence of H_2 as engine load increases. The temperature dependence can be observed in Fig. 7(d), where the mean combustion temperature clearly increases with HES for the same RPM.

The effect of WI on NOx is clearly evident in almost all the Figs. 5 and 6. In fact, a noticeable reduction in NOx is observed with each increase in WI. In Fig. 5(a), with a CR of 17.5 and an HES of 62 %, NOx decreases from 900 ppm without WI to 380 ppm with 0.266 g/cycle of water. This means that water has halved the emission levels. Additionally, in the same figure, at CR 17.5, NOx decreases from 620 ppm at HES 72 % with 0.266 g/cycle of water to 450 ppm at HES 77 % with 0.531 g/cycle of water. In this case, NOx reduces by 50 % with an almost 100 % increase in WI, despite a 7 % increase in HES. Lastly, in the same figure, it can be seen that at CR 16.3 and HES 80 %, NOx emissions decrease from 1050 ppm with 0.531 g/cycle of water to 700 ppm with 0.795 g/cycle of water. In this case, a 33 % reduction in NOx has been achieved with a 50 % increase in WI. A very similar behaviour can be appreciated in the rest of tested conditions.

The procedure by which WI reduces NOx is named the thermal mechanism, where two different mechanisms occur: the first one is the increase in the specific heat of the gases, which reduces the charge temperature during compression and combustion due to the high thermal capacity of water compared to that of the air. The second one is related to the phase change of water; most of the water that enters the cylinder is in a liquid state, although highly atomized. As the compression process advances and the temperature increases, the water undergoes a phase change from a liquid to a gas state, and therefore, it absorbs the energy required for the phase change.

The effect of WI on NOx can also be observed in Fig. 7, which

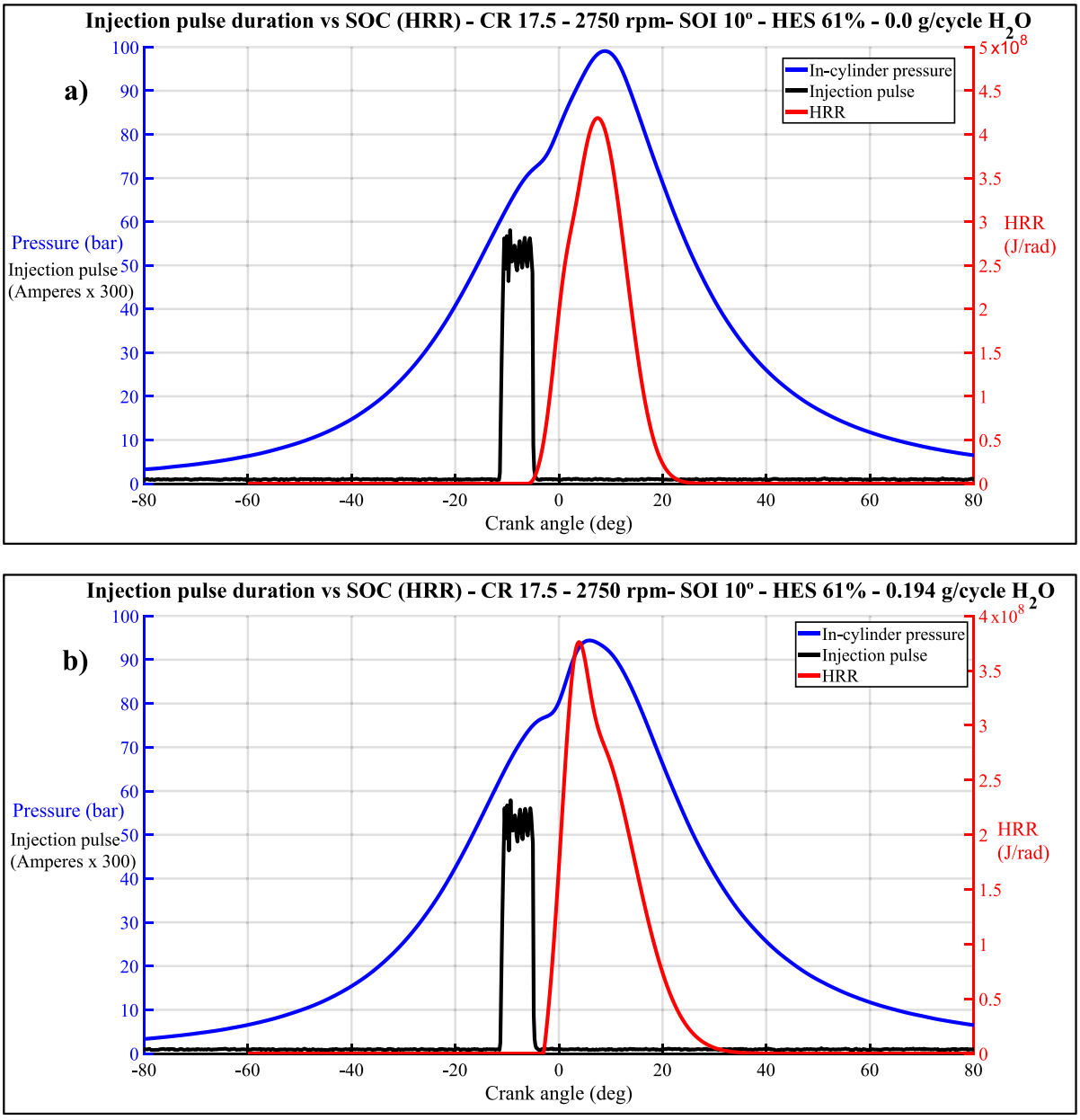

Fig. 4. (a) Comparison of the injection pulse duration and the SOC through the HRR at 2750 rpm and SOI 10° for CR 17.5, HES 61 % and 0.0 g/cycle H_2O. (b) Comparison of the injection pulse duration and the SOC through the HRR at 2750 rpm and SOI 10° for CR 17.5, HES 61 % and 0.194 g/cycle H_2O.

displays the in-cylinder temperature curves for most of the test conditions presented in Fig. 5 and Fig. 6, as modelled by J. Serrano et al. in references [38,39]. Looking at Fig. 7(a) and (b), it is evident that for the same HES, SOI, and CR, any increase in the amount of WI leads to a rapid reduction in temperature evolution and, consequently, in NOx emissions. However, this effect is more pronounced at SOI 5° than at SOI 10°. To put it differently, the higher the SOI, the greater the amount of water required for the same temperature reduction. To emphasize this point, in Fig. 7(a) at HES 62 %, SOI 10°, and CR 16.3, an increase from 0 to 0.266 g/cycle of water results in a reduction of the maximum temperature by almost 70 °C. In Fig. 7(b), at HES 64 %, SOI 5°, and CR 16.3, increasing from 0 to 0.213 g/cycle of water reduces the maximum temperature by almost 120 °C. This is because, with a lower SOI, the maximum temperature inside the combustion chamber is lower, and therefore, with the same thermal capacity of the water (amount of WI per engine cycle), the reduction in temperature is more significant.

Regarding the dependence of NOx on CR, it can be observed in Figs. 5 and 6 that there is an almost linear relationship between CR and NOx. Therefore, the reduction of NOx can be promoted by decreasing CR, regardless of RPM, SOI, or HES. This is because any increase in CR has two effects: it raises the air temperature and shortens the start of combustion (precisely due to the temperature increase). Therefore, reducing CR lowers the gas temperature, deactivating NOx formation. Additionally, the amount of water required to achieve a certain level of NOx is also reduced.

If the effects of both RPM and SOI on NOx formation are analysed for the same amount of H_2 supplied to the engine, a significant reduction in NOx can be observed. When comparing Fig. 5(a) and 6(b) for approximately 20 kW of H_2 and a CR of 16.3, with engine speed ranging from 2000 rpm to 2750 rpm and SOI decreasing from 10° to 5°, the NOx levels decrease from 1050 ppm to 140 ppm, with the latter having a 27 % lower WI. This trend can be observed in the remaining tested conditions, highlighting the cumulative effect of RPM and SOI on NOx reduction.

An analysis of the test data determined the limit for the minimum

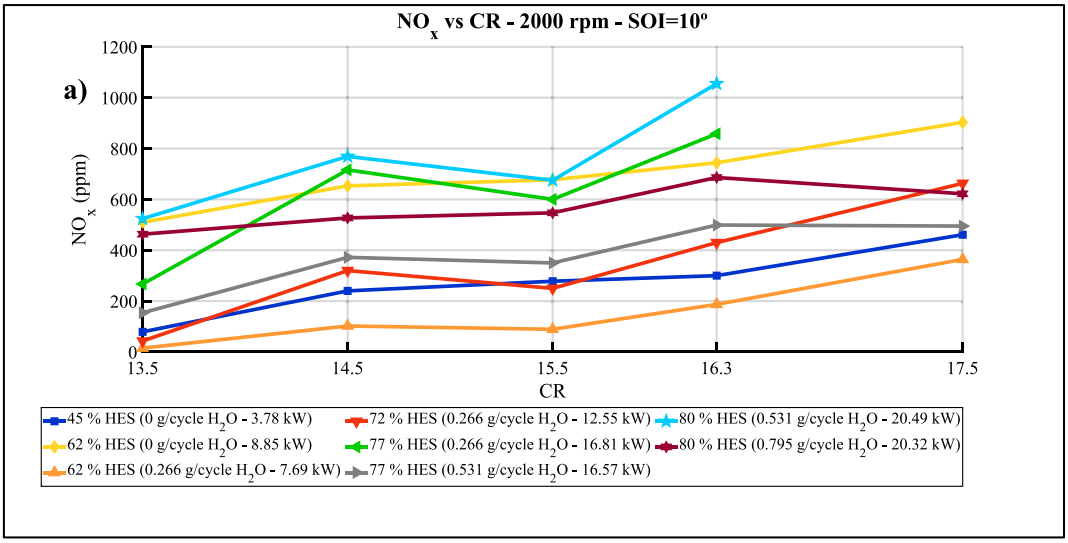

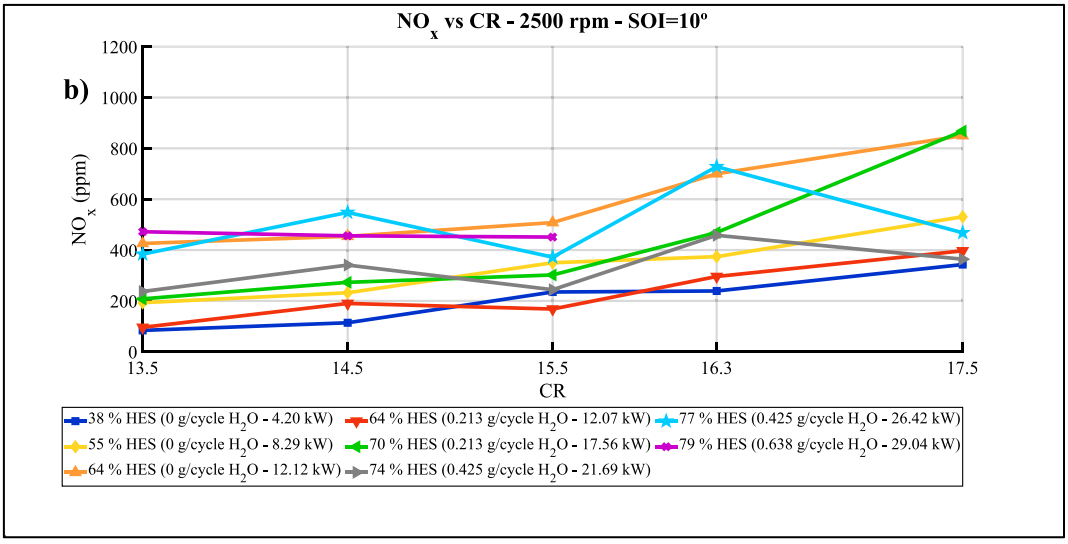

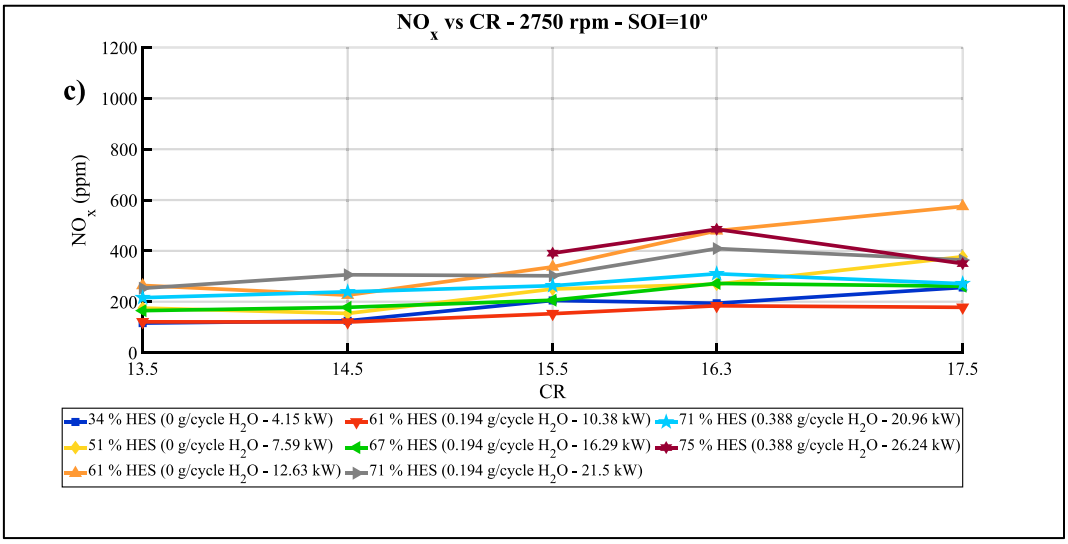

Fig. 5. (a) NO_x emissions versus CR at 2000 rpm and SOI 10° BTDC. (b) NO_x emissions versus CR at 2000 rpm and SOI 10° BTDC. (c) NO_x emissions versus CR at 2750 rpm and SOI 10° BTDC.

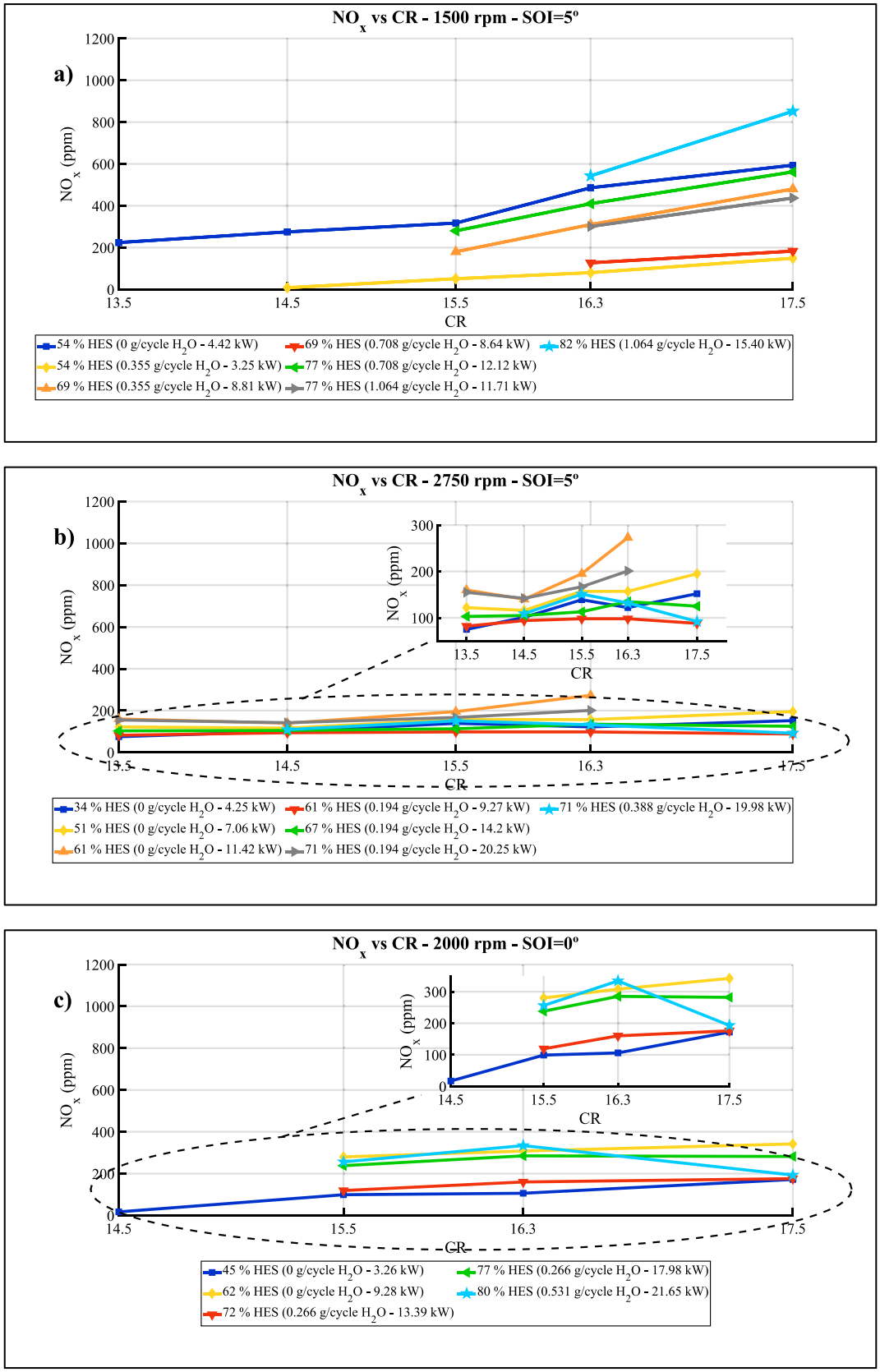

Fig. 6. (a) NO_x emissions versus CR at 1500 rpm and SOI 5° BTDC. (b) NO_x emissions versus CR at 2750 rpm and SOI 5° BTDC. (c) NO_x emissions versus CR at 2000 rpm and SOI 0° BTDC.

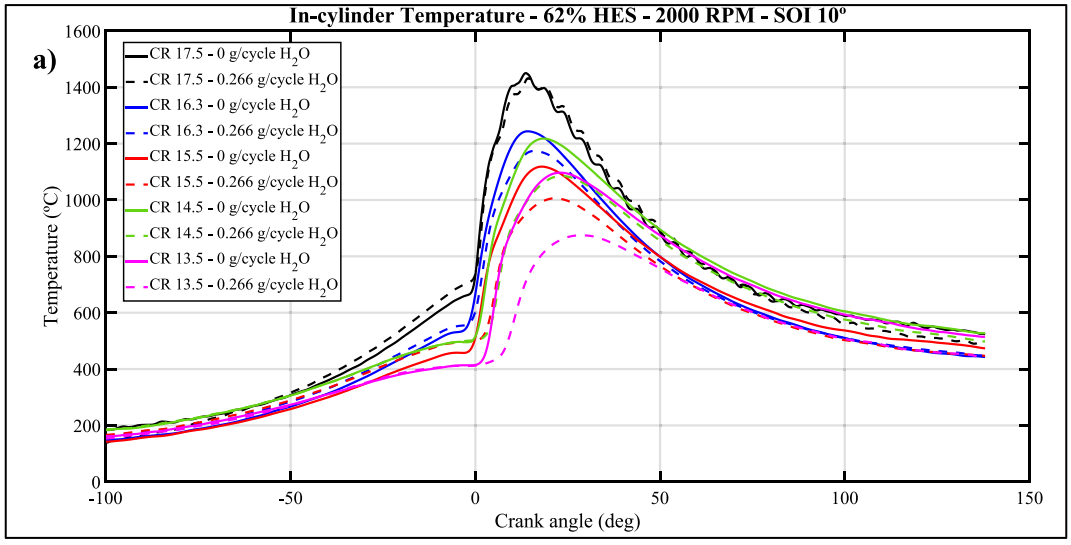

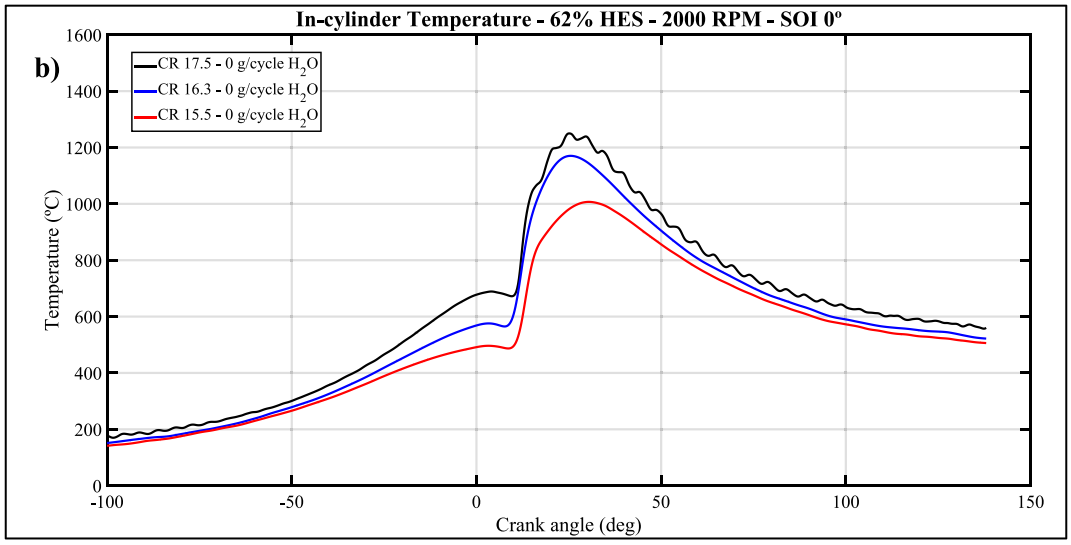

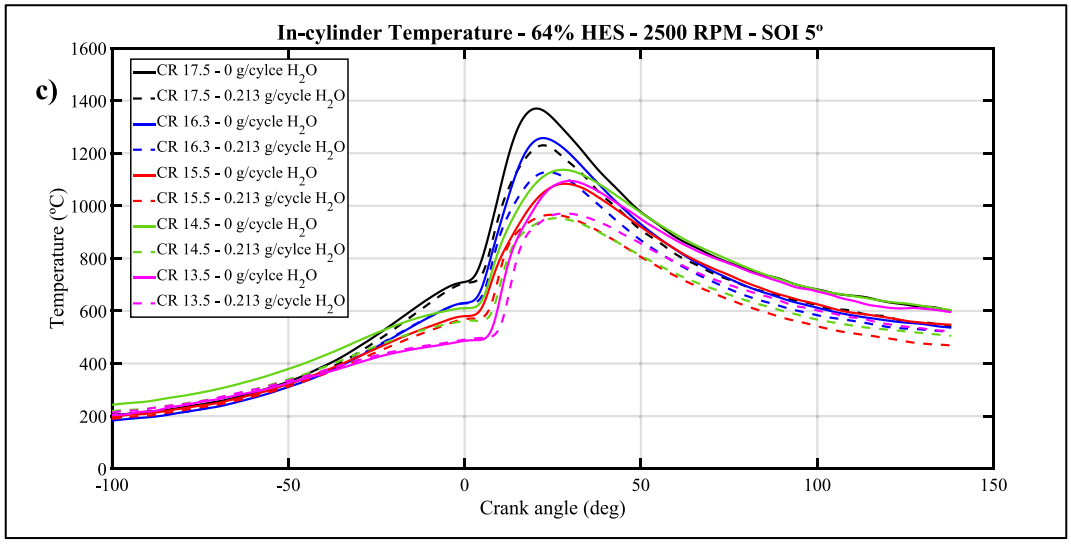

Fig. 7. (a) In-cylinder temperature versus crank angle at 62 % HES, 2000 rpm and SOI 10° BTDC, (b) In-cylinder temperature versus crank angle at 62 % HES, 2000 rpm and SOI 0° BTDC, (c) In-cylinder temperature versus crank angle at 64 % HES, 2500 rpm and SOI 5° BTDC, (d) In-cylinder temperature versus crank angle with variable HES at 2000 and 2500 rpm, SOI 0°, CR 16.3 and without WI.

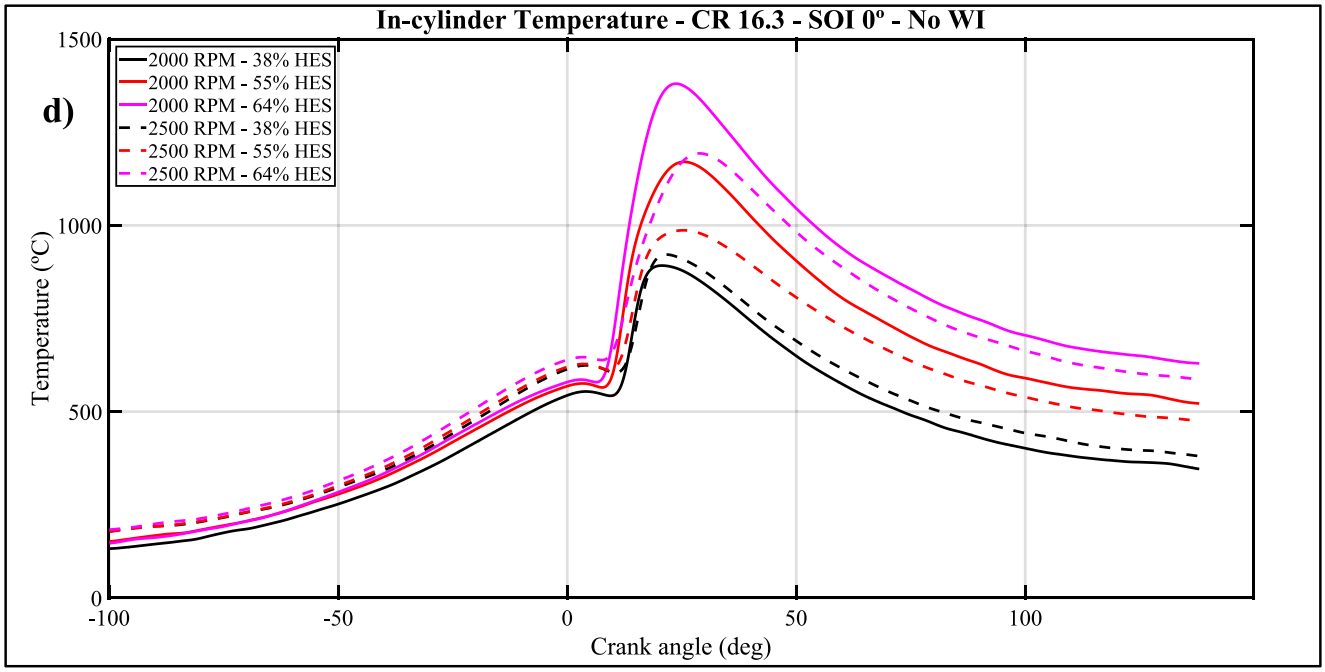

Fig. 7. (*continued*).

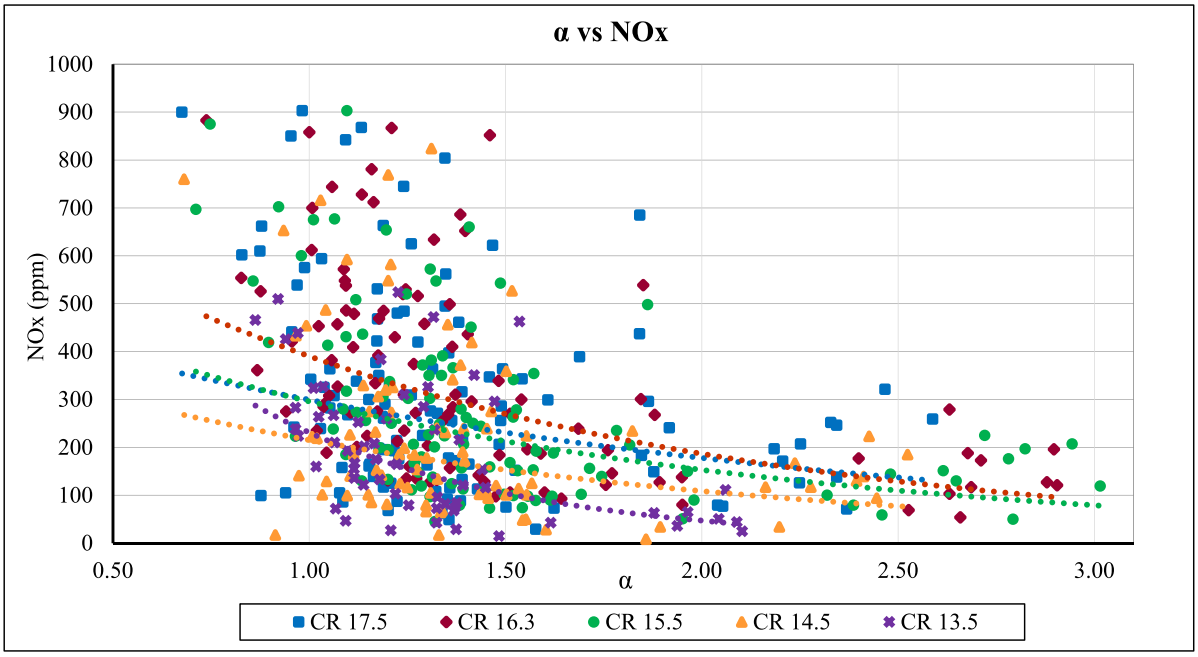

Fig. 8. NO_x versus the parameter α.

attainable NOx emissions, which is related to the thermal capacity of the charge, in this case, air plus water, when referred to the fuel power. This parameter, α, is defined in Equation (2), where T_{Ref} is 300 K:

$$\alpha = \frac{(\dot{m}_{water} \bullet c_{p,water} + \dot{m}_{air} \bullet c_{p,air}) \bullet T_{Ref}}{\dot{m}_{diesel} \bullet LHV_{diesel} + \dot{m}_{H2} \bullet LHV_{H2}} \quad (2)$$

The significance of α is related to NOx emissions, as it represents the relationship between the thermal capacity of the load (comprising air and water) and the power generated by the fuel (diesel + H_2). Both the numerator and the denominator are expressed in the same units, making α dimensionless.

Given the strong temperature-dependent nature of NOx formation, one of the most effective methods to reduce NOx is by increasing the thermal capacity of the charge. In the case of water, which has a specific heat more than twice that of air, it contributes significantly to temperature reduction. Therefore, the parameter α represents the ratio between the agents that decrease charge temperature compared to the total energy released in the combustion chamber.

Fig. 8 illustrates the relationship ~~of~~ between NOx in ppm and the parameter α for all test conditions. For low α, in the range of 1.0–1.5, there is dispersion in the NOx emissions, indicating that multiple factors influence NOx formation, including thermal capacity, residence time, and SOC. However, as the parameter α increases, this dispersion clearly diminishes. When α reaches approximately 2, NOx emissions achieve a

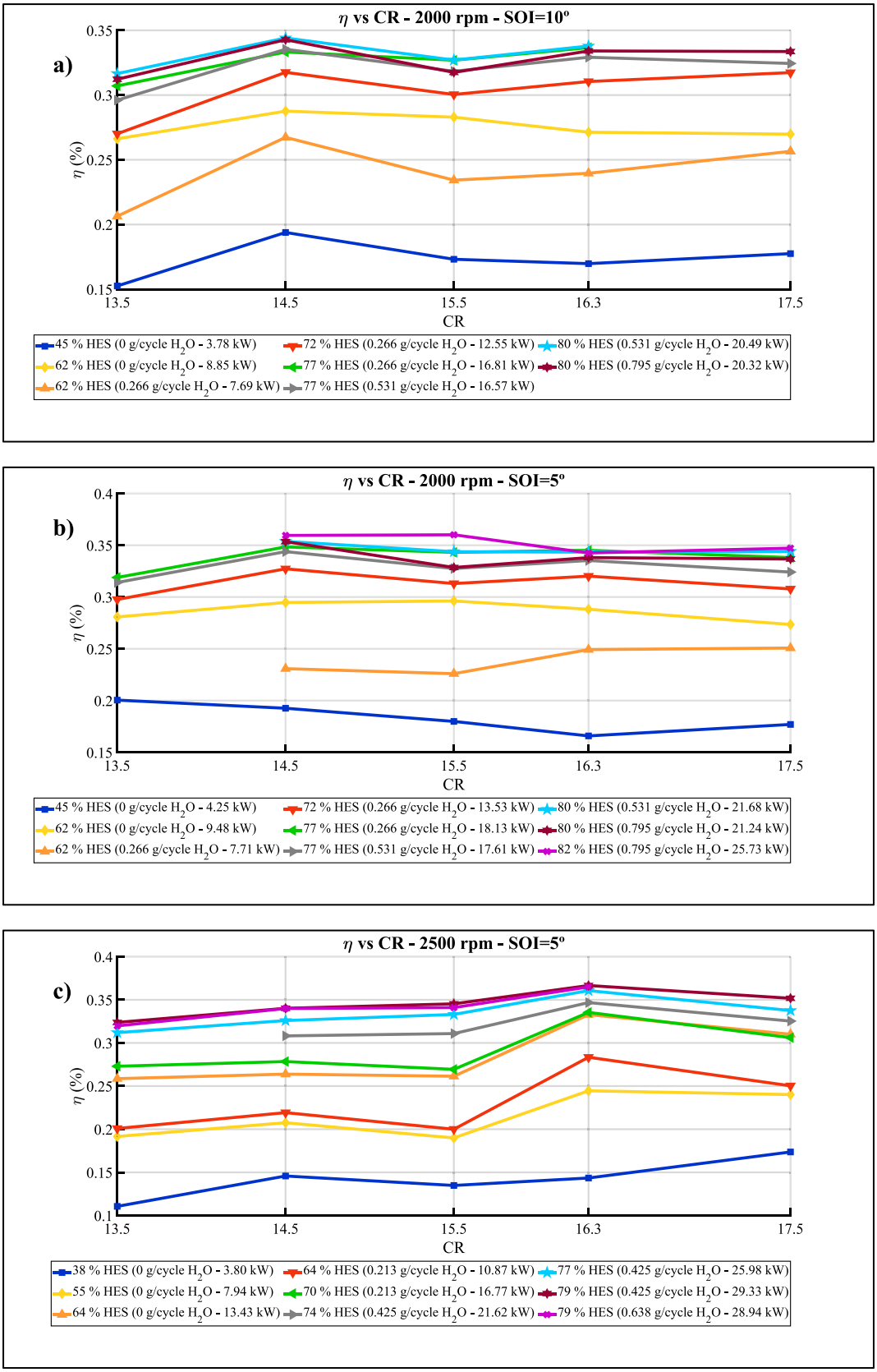

Fig. 9. (a) Efficiency versus CR at 2000 rpm and SOI 10° BTDC, (b) Efficiency versus CR at 2000 rpm and SOI 5° BTDC, (c) Efficiency versus CR at 2500 rpm and SOI 5° BTDC, (d) Efficiency versus CR at 2750 rpm and SOI 10° BTDC.

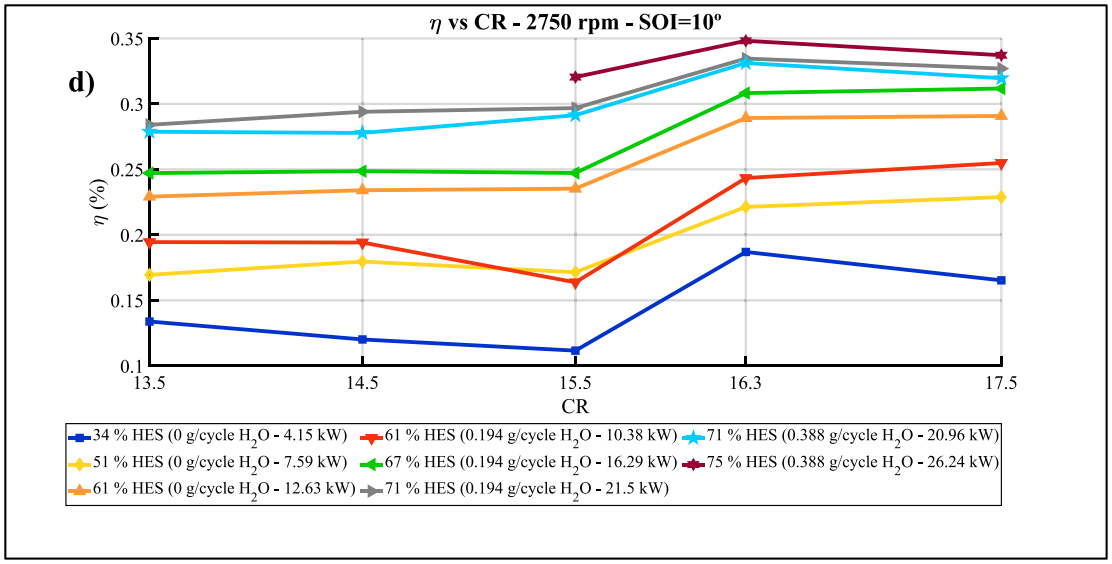

Fig. 9. (*continued*).

minimum in an asymptotic manner, within a range between 200 and 50 ppm for different CRs. This signifies that the thermal mechanism ~~clearly~~ dominates and provides a minimum value for NOx, influenced by the thermal capacity of the load enhanced by water ($Cp_{water} \sim 4\ Cp_{air}$).

From another perspective, Fig. 8 provides insight into the maximum amount of water that can be combined with fuel to achieve the minimum NOx, facilitating the use of this figure in the design of the engine's NOx control strategy. Fig. 8 also illustrates the previously mentioned trends; specifically, the effect of CR on NOx reduction is less pronounced as WI increases. NOx emissions are lowest for CR 13.5:1 (purple line) and highest for CR 17.5:1 (blue line), as higher CR results in a more significant increase ~~of~~ in combustion chamber temperature. On average, a reduction of 50–60 % in NOx emissions is achieved by decreasing the CR from 17.5:1 to 13.5:1. This trend can be observed in Fig. 8 through the different lines representing NOx emissions for each CR value.

4.2. Effect on the efficiency

Equation (3) demonstrates how efficiency (η) is evaluated:

$$\eta = \frac{2 \bullet \pi \bullet N \bullet Torque}{\dot{m}_{diesel} \bullet LHV_{diesel} + \dot{m}_{H2} \bullet LHV_{H2}} \tag{3}$$

As can be seen in Fig. 9, efficiency increases with increasing HES and reaches its maximum when HES exceeds 70 % for all CR and test conditions. For all CR values, when the HES falls within the range of 40 %–80 %, efficiency ranges between 0.15–0.35. The differences in efficiency among different RPM and SOI conditions are very small, approximately 2 %, when HES and H_2O mass flow remain constant. This can be observed in Fig. 9 when comparing points with the same HES and water mass flow. For example, in the case of 80 % HES and 0.531 g/cycle (H_2O mass flow per cycle), efficiency ranges between 0.34 and 0.36 for different RPM and SOI conditions, all at the same CR.

Efficiency exhibits an almost flat trend between CR 17.5 and 14.5, while for CR 13.5, the efficiency is lower, decreasing from 0.35 to 0.30, for instance. This trend is observed under various HES, RPM, and SOI conditions.

As it is very well known in the theoretical internal combustion engine cycle model, the higher the CR, the higher the efficiency, although for high CR, the increase in efficiency slows down. When considering real cycle effects such as mass and mechanical losses, which increase with CR, it is evident that there is an optimal CR. In this experimental analysis, it is obvious that within the range of 14.5–17.5, the efficiency remains almost constant but decreases significantly below 14.5.

Conversely, efficiency decreased significantly with an increase in the quantity of H_2O. This can be observed in Fig. 9(a) and (b) for the yellow line (62 % HES and 0.0 g/cycle H_2O) and the orange one (62 % HES and 0.266 g/cycle H_2O), with a maximum drop in efficiency of 5 %. This drop is independent of the operating conditions, as the same trend is observed in Fig. 9(d) between the orange and the red lines. The reduction in efficiency can be attributed to the temperature decrease resulting from the extended combustion duration, which leads to a deviation from constant-volume combustion in the combustion process. Furthermore, this extended duration increases the time available for heat losses.

The increase in HES results in higher NOx emissions, as shown in section 4.1, but it also leads to improvements in efficiency and MEP. Fig. 10 illustrates the MEP trends with increasing HES, ranging from CR 13.5:1 to 17.5:1. For the same HES, a consistent trend is observed in the MEP curves, indicating that there is no penalty associated with reducing the CR. These trends suggest that achieving stable and knock-free combustion in an H_2-fueled engine is possible even at lower CR levels with high HES levels. As anticipated, the maximum MEP values are achieved at high HES levels across all CR conditions. In contrast to efficiency, a reduction in CR does not significantly affect impact MEP.

It can also be observed that WI results in a maximum MEP loss of 0.5 bar compared to cases without WI or with a lower amount of H_2O, under the same HES and operational conditions. This can be seen, for example, in Fig. 10(a) between the yellow line (62 % HES and 0 g/cycle of H_2O) and the orange one (62 % HES and 0.266 g/cycle of H_2O), as well as the green line (77 % HES and 0.266 g/cycle of H_2O) compared to the grey one (77 % HES and 0.531 g/cycle of H_2O). This trend is also evident in Fig. 10(b) between the orange line (64 % HES and 0 g/cycle of H_2O) and the red one (64 % HES and 0.213 g/cycle of H_2O). This implies that there is a penalty associated with ~~the~~ WI or increasing the water amount in the MEP values, regardless of the HES, CR, or operational conditions.

4.3. Effect on the start of combustion angle (SOC)

Fig. 11 illustrate the evolution of SOC versus CR at different SOI and RPM, while taking into account HES and WI as parameters. Meanwhile, Fig. 14 depict the calculated HRR versus crank angle, considering various CR, RPM, and SOI values and incorporating HES and WI as parameters.

The first parameter that affects SOC is RPM. As engine speed increases, and because the combustion angle remains constant, there is a reduction in the available time for combustion. Despite RPM promoting combustion velocity through turbulence, it is not sufficient, and

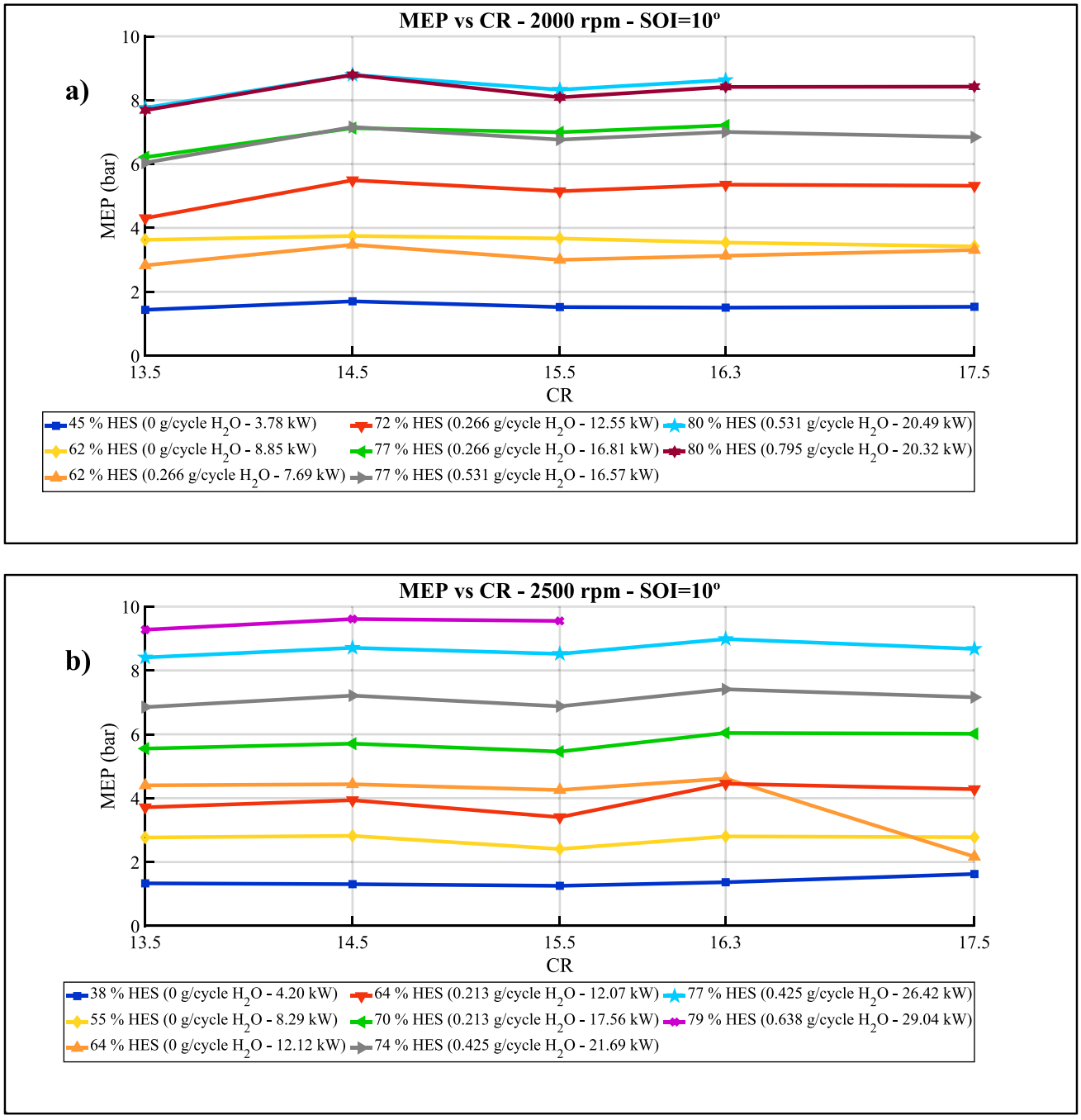

Fig. 10. (a) MEP versus CR at 2000 rpm and SOI 10° BTDC. (b) MEP versus CR at 2500 rpm and SOI 10° BTDC.

ultimately, SOC is delayed with higher RPM.

This trend is clearly observable at SOI 5° in Fig. 11(b), (c), and (d), where under all CR and test conditions, SOC consistently increases with RPM. To provide clarity, let's focus on the test condition without WI and with the same HES (represented by the dark blue line). At a CR of 13.5, SOC increases from 5° at 1500 rpm to 8.3° at 2750 rpm. When the CR is increased to 17.5, SOC increases from −0.3° at 1500 rpm to 3° at 2750 rpm. This behaviour is also evident when comparing Fig. 11(a) and (e) for SOI 10°.

The dependence of SOC on HES can be observed when we exclude the effects of WI; therefore, only the cases with 0 g/cycle of water are considered here. When examining Fig. 11(c) (2500 rpm and SOI 5°) and comparing HES levels of 38 %, 55 %, and 64 % for CR 13.5, SOC decreases from 7° to 6° to 5°, respectively. In the same Fig. 11(c), for CR 15.5, SOC steadily decreases from 5° at 38 % HES to 2.2° at 64 % HES in an almost linear fashion. Finally, in the same Fig. 11(c) at CR 17.5, SOC goes from 3.5° to 2.1° to 1.0° for HES 38 %, 55 %, and 64 %, respectively.

Fig. 14 displays the HRR curves for most of the test conditions presented in Fig. 11, as modeled by J. Serrano et al. in references [38,39]. In this Fig. 14(a) (CR 17.5 and 2000 rpm), it is clearly demonstrated that an increase in HES results in a reduction in SOC. Firstly, the area of HRR increases with HES because of the increased amount of H_2, and at the same time, the maximum of the HRR also rises, raising gas temperature. This is the main factor responsible for SOC reduction; as temperature increases within the combustion pressure range, the kinetics of the fuel that produces autoignition accelerates. Therefore, this continuous reduction in SOC with HES is attributed to the increase in combustion

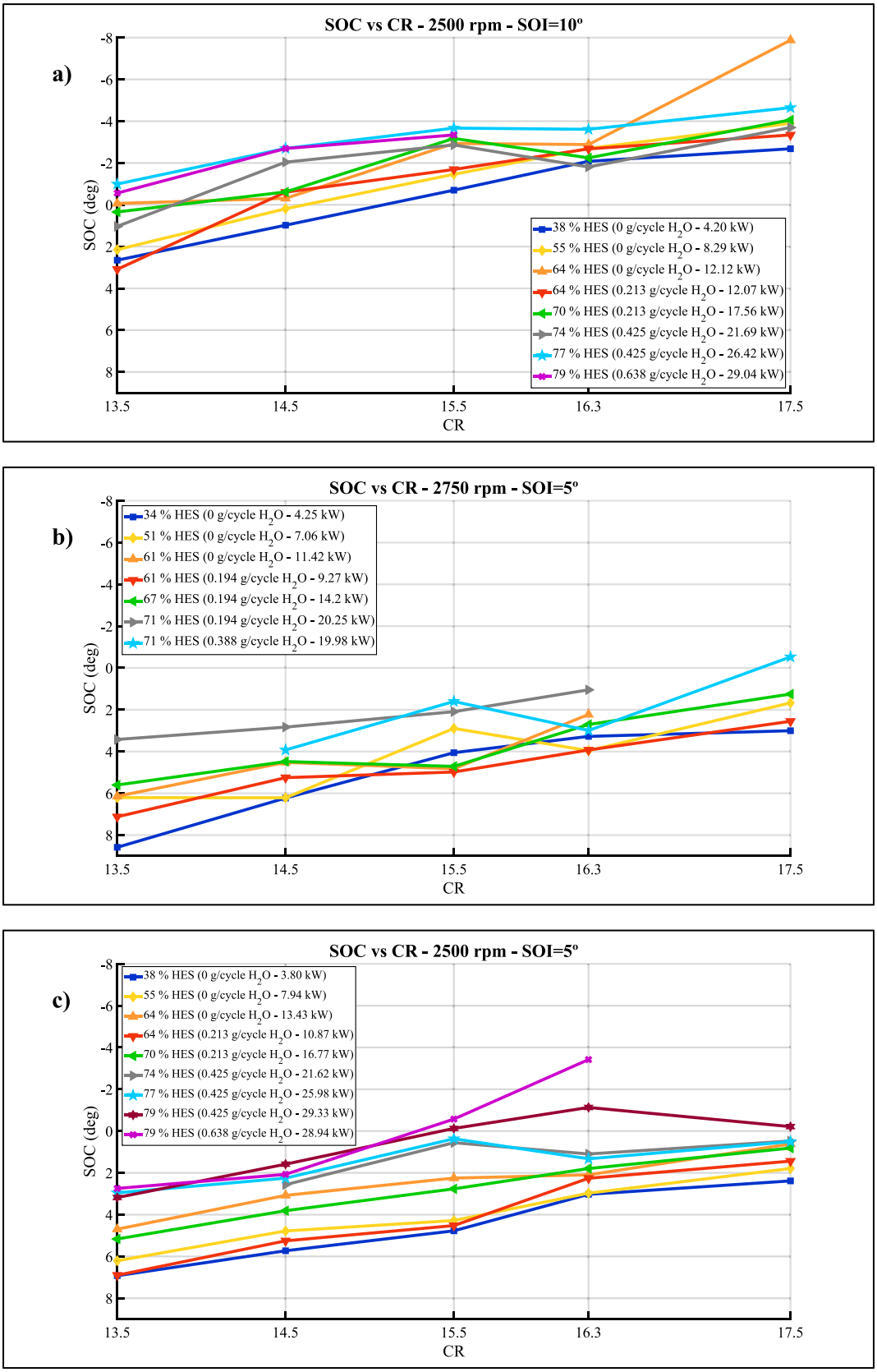

Fig. 11. (a) SOC versus CR at 2500 rpm and SOI 10° BTDC, (b) SOC versus CR at 2750 rpm and SOI 5° BTDC, (c) SOC versus CR at 2500 rpm and SOI 5° BTDC, (d) SOC versus CR at 1500 rpm and SOI 5° BTDC, (e) SOC versus CR at 2750 rpm and SOI 10° BTDC.

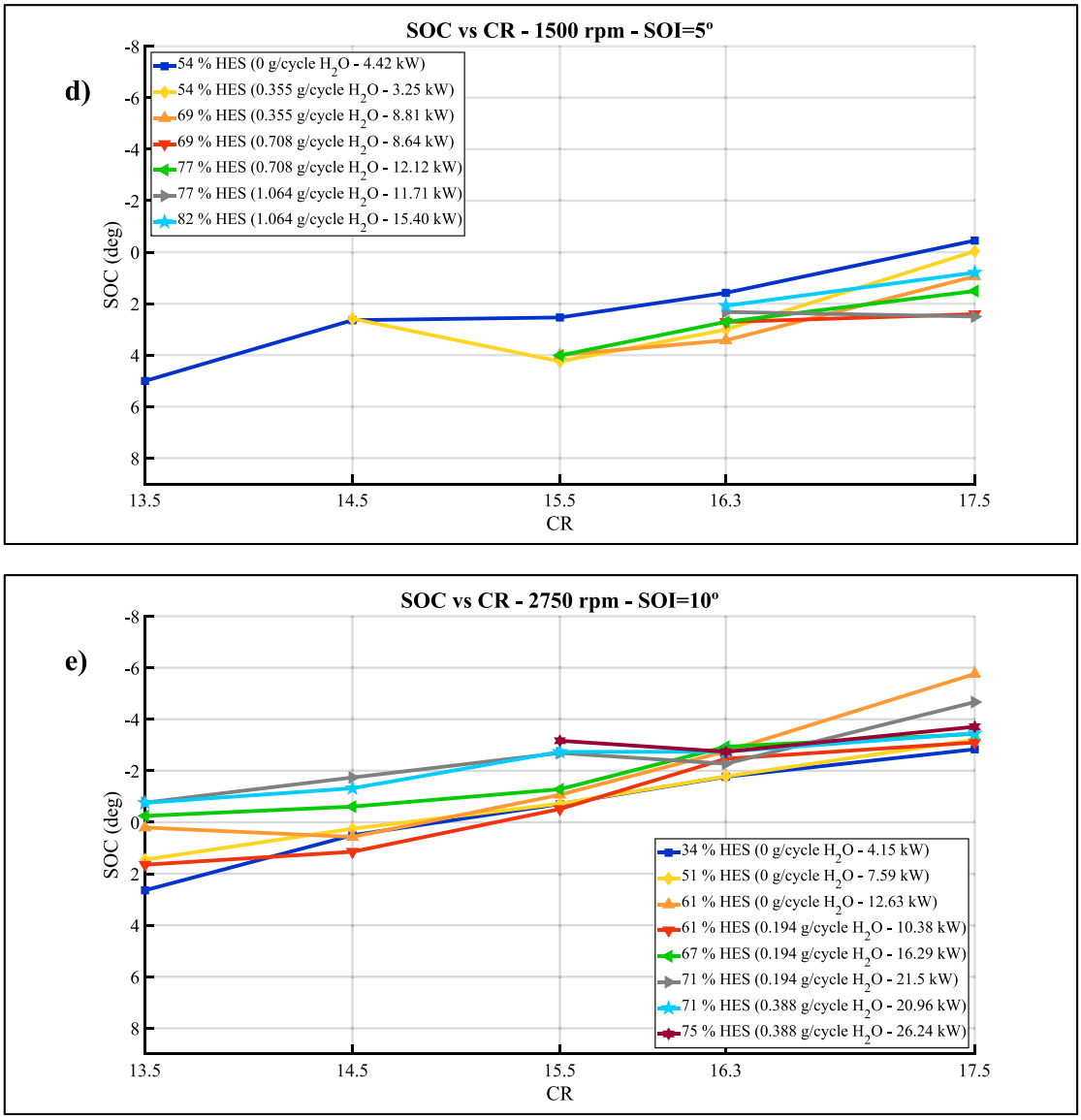

Fig. 11. (*continued*).

gas temperature due to the greater presence of H_2 as engine load increases at the same RPM. Although the specific heat at constant pressure of H_2 is significantly higher compared to that of air roughly fourteen times greater, to be precise the low mass of H_2 leads to a continuous increase in gas temperature with an increase in engine load.

The effect of WI on SOC can be observed in almost all of Fig. 11(a)–(e). For the same HES, the higher the WI, the higher the SOC. This is due to the temperature reduction caused by the presence of water in the gases, which delays the start of combustion. In Fig. 11(a) (2500 rpm and SOI 10°) with HES 64 % and CR 13.5, SOC increases from 0° without WI to 3° with WI of 0.213 g/cycle of water. At CR 17.5 and HES 64 %, SOC changes from −8° without WI to −3° with 0.213 g/cycle of water. When looking at HRR, the dependence of SOC on WI is clearly evident in a physical context. In Fig. 14(b) (CR 16.3, 2000 rpm and SOI 10°) at HES 77 %, SOC goes from −3.6° to −3.0° as WI increases from 0.266 g/cycle to 0.531 g/cycle, respectively. Moreover, at HES 80 %, the SOC changes from −4.3° to −3.2° with an increase in WI from 0.531 g/cycle to 0.795 g/cycle, respectively. In this Fig. 14(b), it can be seen that not only is SOC delayed as WI increases for the same HES, but the maximum of the HRR also shifts roughly by the same angle. In other words, the entire combustion process is delayed along with SOC. A very similar behaviour is observed in Fig. 14(c) (CR 15.5, 2000 rpm and SOI 10°) at HES 77 %, where SOC goes from −1° to 0° as WI increases from 0.266 g/cycle to 0.531 g/cycle, respectively. Moreover, at HES 80 %, the SOC changes from −2° to 3° with an increase in WI from 0.531 g/cycle to 0.795 g/cycle, respectively. As seen, the SOC is delayed by approximately 1° for an increase in WI of around 100 %, although the initial angle depends on the CR.

Regarding the dependence of SOC on CR, it can be observed from Fig. 11 that there is an almost inverse relationship between CR and SOC: the higher the CR, the lower the SOC. Therefore, an increase in CR results in a reduction of SOC, regardless of RPM, SOI, WI, or HES. This is because any increase in CR raises the air temperature and shortens the temporal history of the fuel that controls the start of combustion within the pressure range.

4.4. *Effect on the in-cylinder maximum pressure*

The maximum pressure inside the combustion chamber is of great interest because it affects the mechanical integrity of the engine. As mentioned in section 3, the specific power of the engine is limited not only by knock but also by mechanical constraints. Therefore, in this

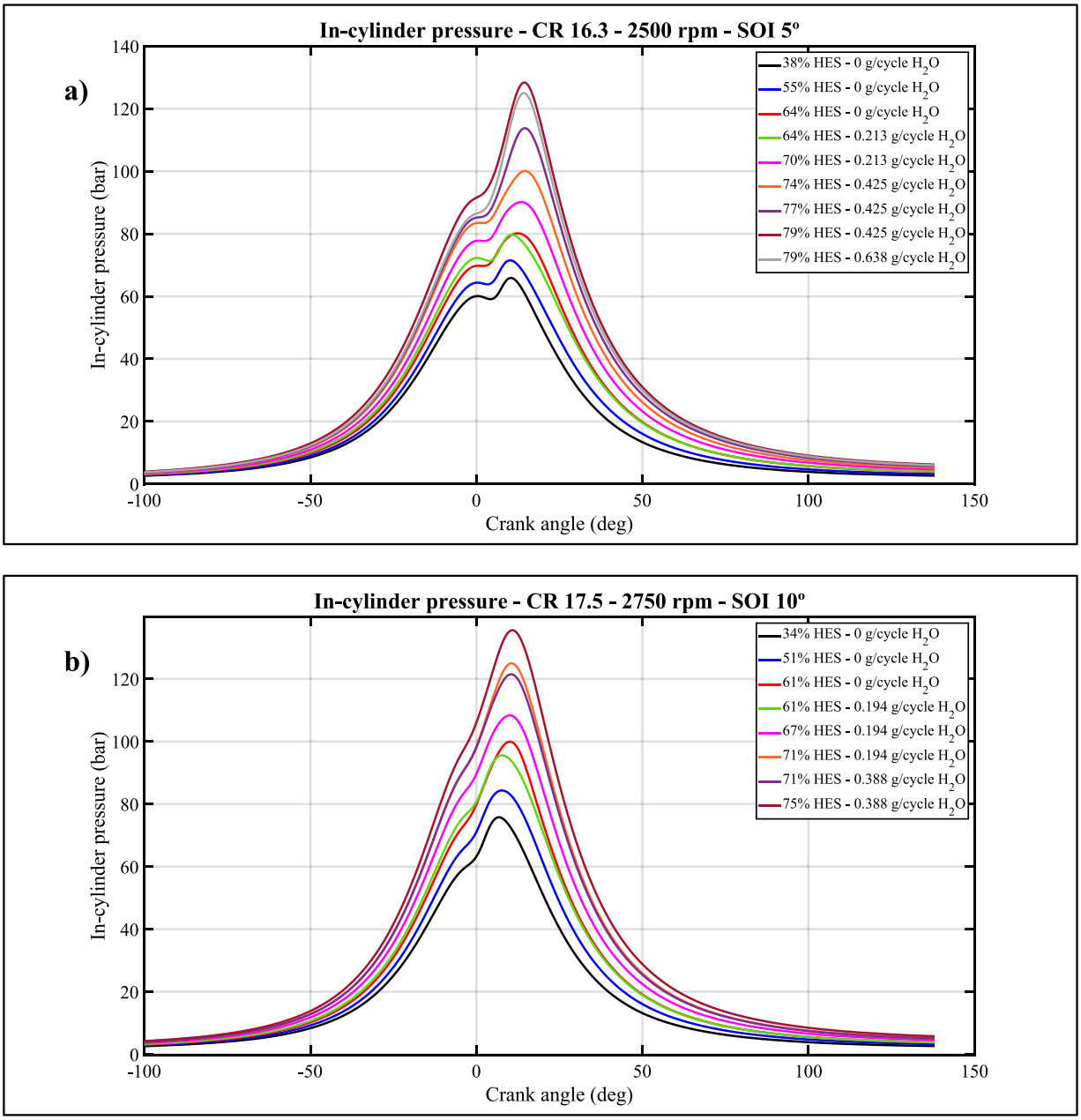

Fig. 12. Combustion pressure at different HES and WI. (a) CR 16.3, SOI 5° and 2500 RPM, (b) CR 17.5, SOI 10° and 2750 rpm.

section, the factors that control peak pressure in dual combustion are identified.

Fig. 12(a) and (b) depict combustion pressure versus crankshaft angle for various testing conditions. Common observations from both figures are as follows:

- The higher the HES, the greater the pressure at the end of compression and also the maximum pressure. This is attributed to the increased pressure ratio of the compressor with engine load, resulting in higher intake pressure. This trend is evident for any CR, WI, SOI, or RPM.
- Increasing WI has only a marginal effect on reducing the maximum pressure. The pressure is more responsive to an increase in HES than to an increase in WI.

To delve deeper into the subject, changes in the maximum in-cylinder pressure can be observed in Fig. 13(a) to (e). These figures illustrate the trends in maximum in-cylinder pressure with increasing HES, ranging from a CR of 13.5:1 to 17.5:1.

For the same HES and H_2O content, there is an observed increase of between 20 and 40 bar in pressure from CR = 13.5 to CR = 17.5. This trend holds true across all operational conditions and HES ranges. For instance, in Fig. 13(b), for the red line representing 72 % HES and 0.266 g/cycle H_2O, the maximum pressure at CR = 13.5 is 60 bar, while at CR = 17.5, it reaches 100 bar. Conversely, in Fig. 13(d), for the orange line with 63 % HES and 0.0 g/cycle H_2O, the maximum pressure at CR = 13.5 is 65 bar, and at CR = 17.5, it reaches 85 bar. This indicates a continuous increase in maximum pressure with increasing CR. This behavior is valuable as it demonstrates that any CR increase exacerbates the mechanical load on the engine, which is contrary to the perspective of enhancing engine efficiency.

WI also leads to a reduced drop in in-cylinder pressure. If you observe Fig. 13(b), there is a 5-bar difference between the yellow line (62 % HES and 0.0 g/cycle H_2O) and the orange one (62 % HES and 0.266 g/cycle

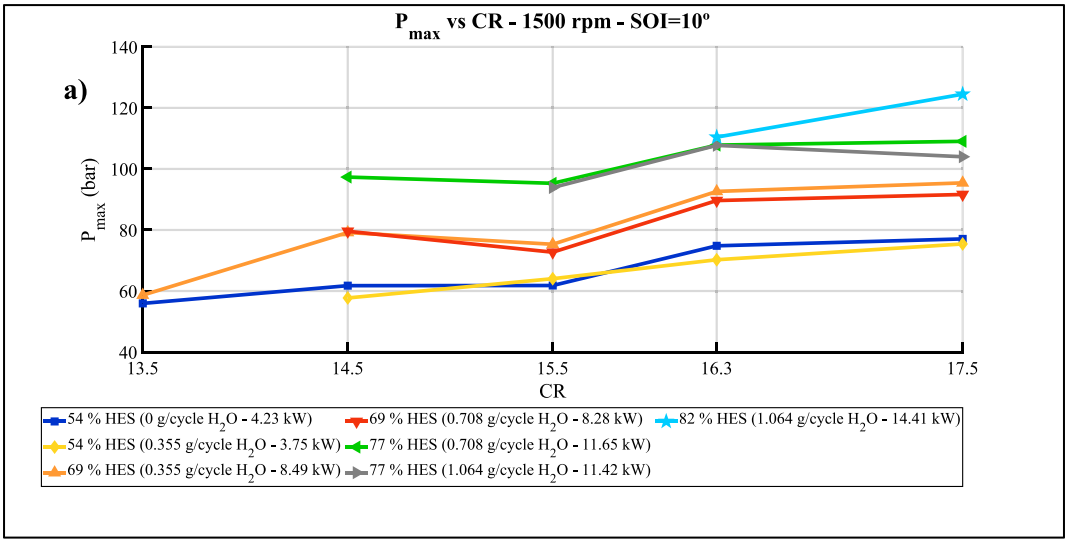

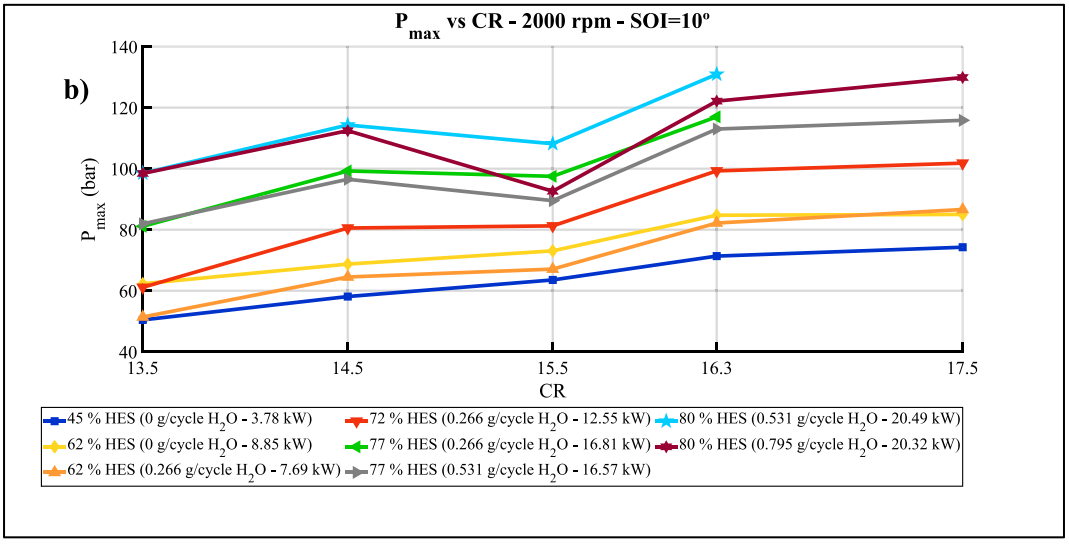

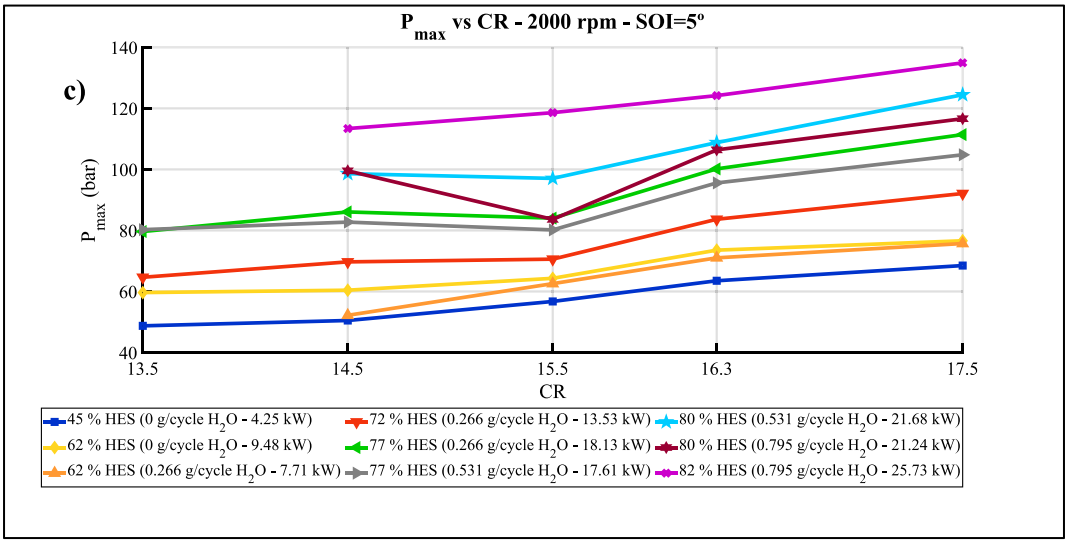

Fig. 13. (a) In-cylinder maximum pressure versus CR at 1500 rpm and SOI 10° BTDC, (b) In-cylinder maximum pressure versus CR at 2000 rpm and SOI 10° BTDC, (c) In-cylinder maximum pressure versus CR at 2000 rpm and SOI 5° BTDC, (d) In-cylinder maximum pressure versus CR at 2500 rpm and SOI 5° BTDC, (e) In-cylinder maximum pressure versus CR at 2750 rpm and SOI 10° BTDC.

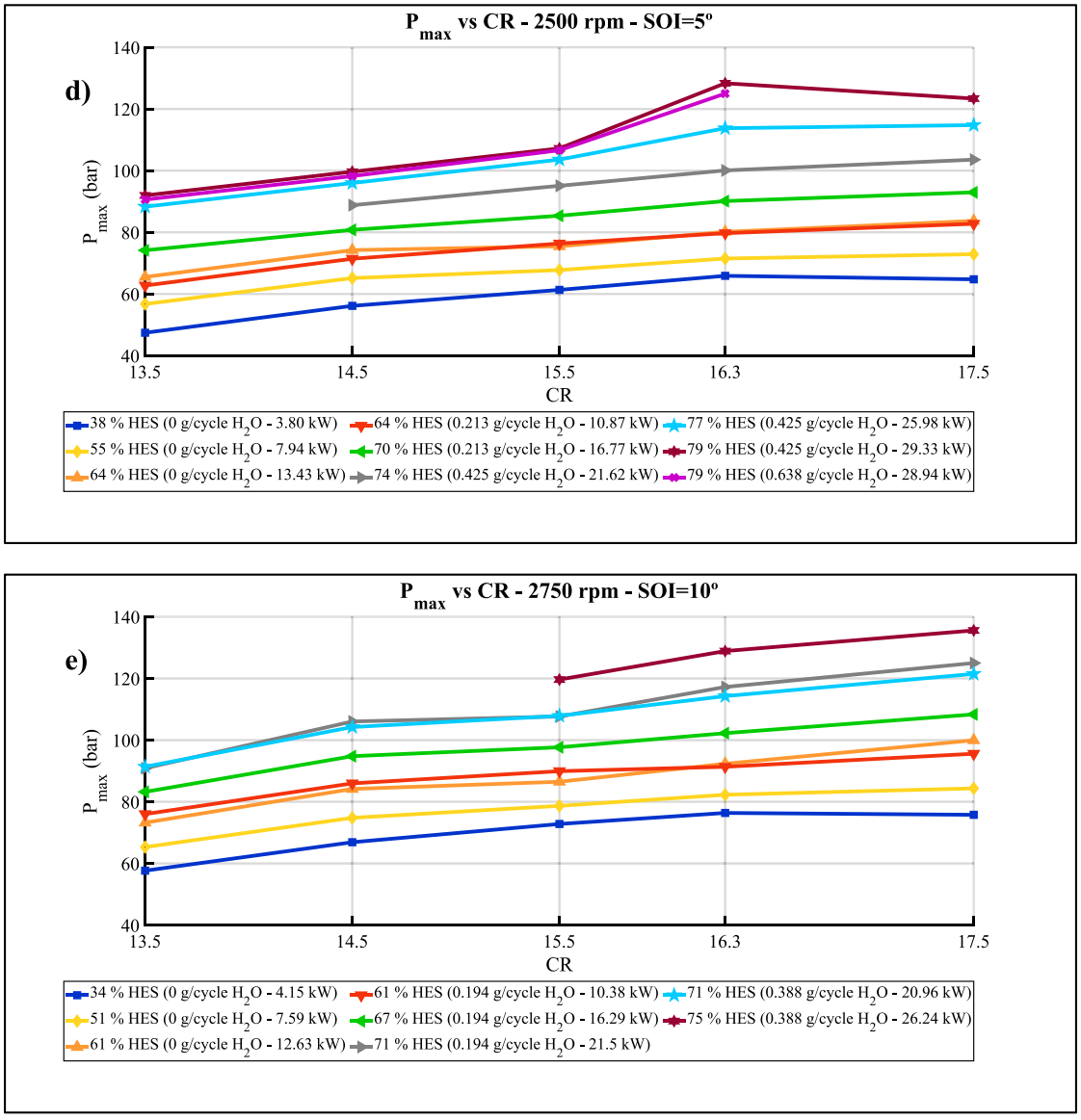

Fig. 13. (*continued*).

H_2O). This trend is consistent across all CR values and operational conditions. A similar decrease in ~~the~~ pressure can be observed in Fig. 13 (e) between the orange and red lines. The maximum pressure drop due to WI or an increase in its quantity ranges between 5 and 10 bar.

5. Analysis of the HRR

The observed changes in HRRs with CR, SOI, HES, and WI justify a deep analysis based on the HRR. From Fig. 14(a)–(b), experimental HRRs are depicted for most of the tested conditions. When analyzing their shapes, the HRRs can be categorized into three groups: single mode (SM), single mode with partial low rate (SML), two modes (TM).

Due to the complexity of the combustion process and the need for comprehensive explanation, a Computational Fluid Dynamics (CFD) approach has been employed to simulate the three observed combustion modes while maintaining the same conditions as those measured in the tests. The simulation was conducted using Ansys-FORTE 2022 R2, specialized software designed for internal combustion engines. The combustion process has been solved by applying axial symmetry to tested conditions, and the combustion chamber, with the same geometry as the piston for CR 17.5:1, has been divided into 8 sectors. Fig. 15 shows the temperature field output for three of the tested conditions, representative of the HRRs shapes, all of them at CR 17.5:1 and 2000 rpm, where the temperature scale is different for every picture. The presented crankshaft angles are −5°, −2°, 0°, +5°, +10°, and + 20°.

Since H_2 is supplied through the intake port along with the air, it is assumed that the fuel has had sufficient time (~360° referred to the crankshaft angle) to thoroughly mix with the air, resulting in an almost homogeneous fuel–air equivalence ratio throughout the combustion chamber.

From the experimental HRRs, the combustion process is explained:

- SM, where the HRR is fully dominated by a single pulse associated with a premixed combustion process. In this case, once SOC is achieved, the energy of the fuel is released progressively, burning in a single step in a continuous fashion. These are the cases shown in Fig. 14(a) with HES 0 % (only diesel fuel to maintain RPM), Fig. 14 (b) with HES 77 % (magenta) and 80 % (orange), both with WI, and Fig. 14(c) with HES 80 % and WI. In this mode, there is only one relative maximum of the HRRs, and the shape is almost symmetrical around a vertical line that passes through the maximum, that increases almost linearly with HES, irrespective of the presence of

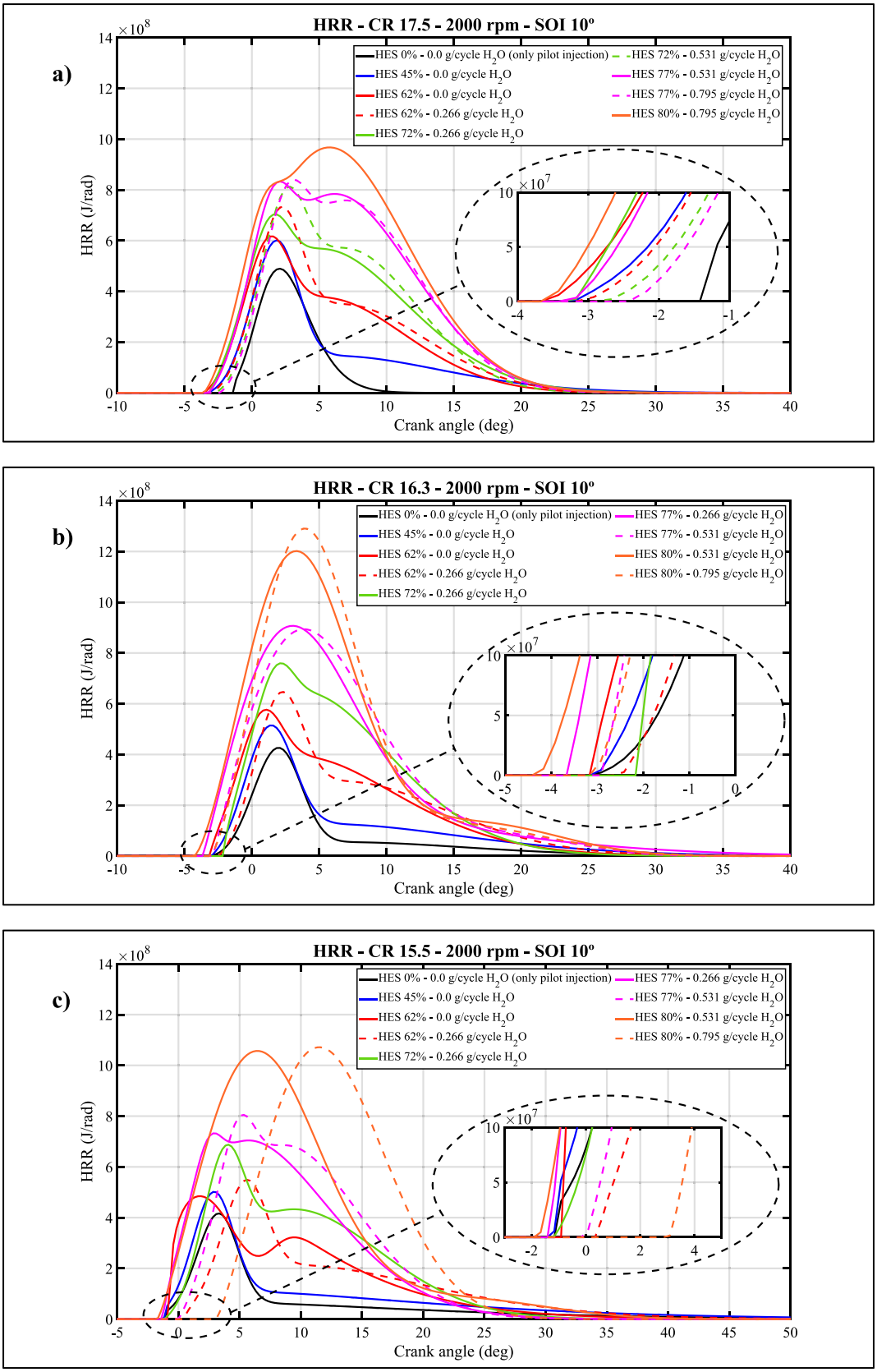

Fig. 14. (a) HRR at CR 17.5, 2000 rpm and SOI 10° with different HES and H_2O flow (b) HRR at CR 16.3, 2000 rpm and SOI 10° with different HES and H_2O flow, (c) HRR at CR 15.5, 2000 rpm and SOI 10° with different HES and H_2O flow, (d) HRR at CR 14.5, 2000 rpm and SOI 10° with different HES and H_2O flow, (e) HRR at CR 13.5, 2000 rpm and SOI 10° with different HES and H_2O flow.

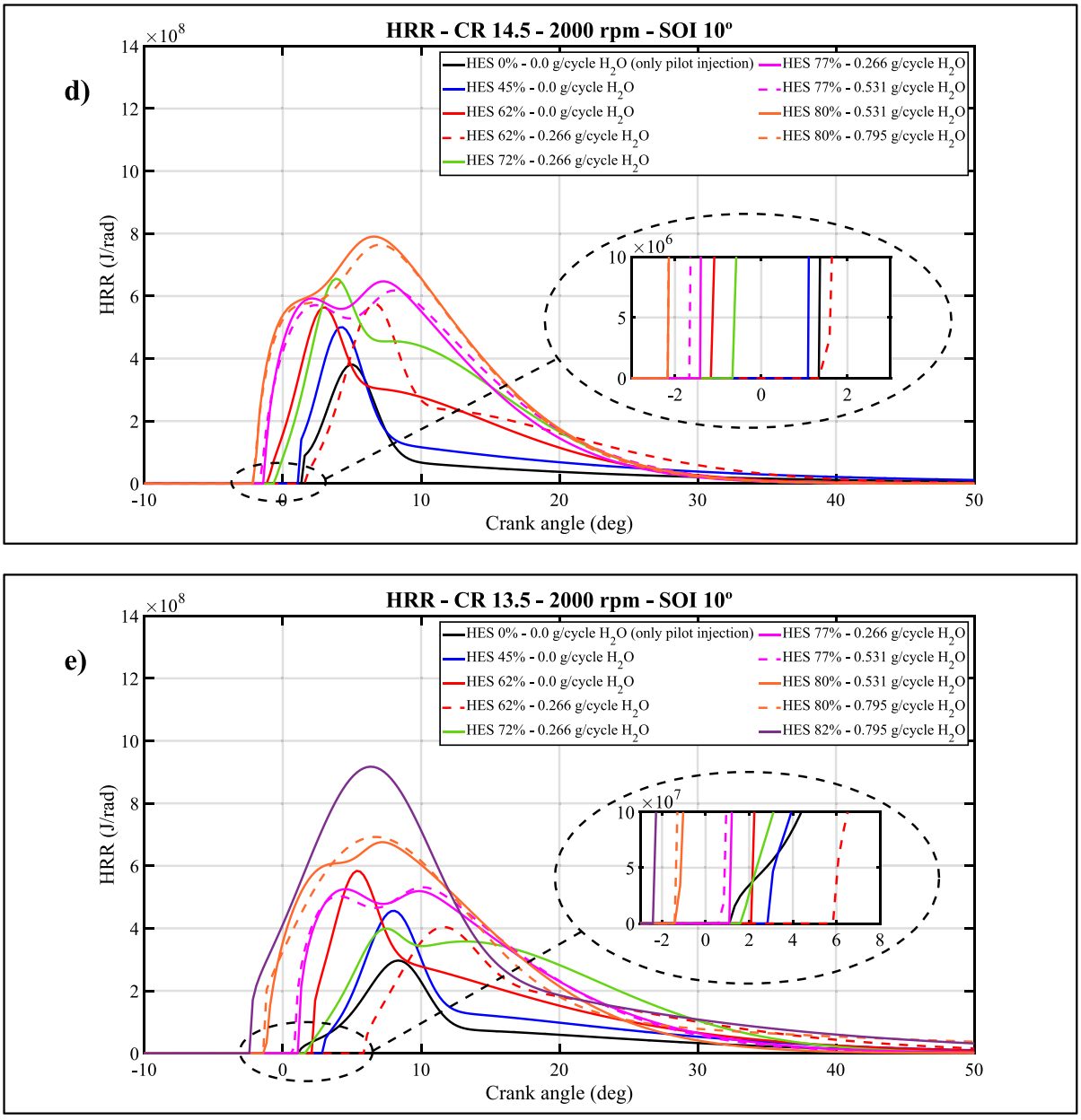

Fig. 14. (*continued*).

water. This combustion mode occurs at very low loads (only pilot injection) and at the highest loads supported by H2, regardless WI and CR.

- SML. In this case, combustion appears to partially resemble a premixed mode, with only one relative maximum in the HRR, but a substantial portion of the fuel is burned at low speeds, extending the combustion duration. These cases are illustrated in Fig. 14(a)–(e) for HES 45 % (blue) without WI and for HES 62 % with and without WI (red). The shape of the HRR has deviated from being symmetrical, and in terms of liberated energy, this segment of the HRR accounts for approximately 50 %. Therefore, it is likely to contribute to a reduction in combustion efficiency and potentially an increase in the amount of unburnt H2. Nonetheless, the maximum HRR increases with HES in an almost linear fashion. This combustion mode primarily occurs at medium loads, within a range of 45 %–77 % HES, although it is influenced by CR. Similar to the other combustion mode, WI has no impact on the shape of the HRR and only causes a delay in the SOC.
- TM, where HRRs exhibit two relative maxima that define a dual combustion mode. This occurs in cases where the HES is above ~ 70 %, typically at medium–high loads, as can be observed in Fig. 14(a)–(e). For medium loads, the first HRR maximum is greater than the second one, but for higher HES values, the second maximum exceeds the first, and the energy liberated under this second combustion mode is also higher. This combustion mode primarily occurs at lower compression ratios, ranging from 15.5:1 and below. It also manifests at medium to high loads, specifically within the range of 62 % to 80 % HES. WI alters HRR by delaying the SOC, but it does not significantly change the HRR's shape.

From the temperature field provided by the simulation in Fig. 15, the combustion processes are compared:

The first point to consider is the different SOC. At −5°, combustion has not started in any mode, but at −2°, the temperature field has changed significantly. The SML exhibits the highest temperature, indicating that the SOC is at its minimum, as shown in Fig. 14(a). At this

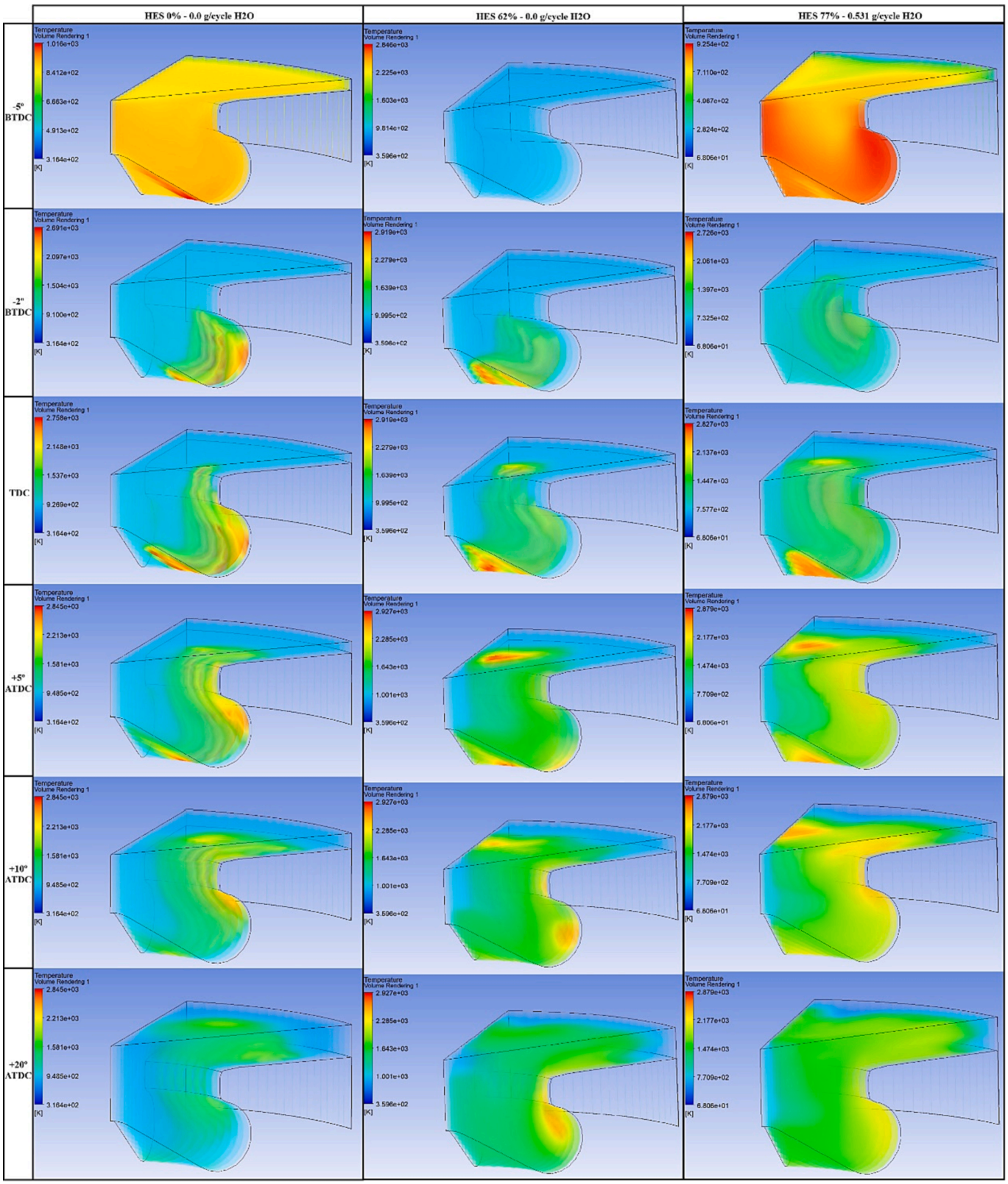

Fig. 15. Temperature evolution at 2000 rpm and SOI 10° at −5°, −2°, 0°, +5°, +10°, +20°. A) HES 0 % SM, B) HES 62 % SML, C) HES 77 % with WI, TM.

angle, the effect of WI is also evident. Despite the higher amount of H_2 in the TM, the temperature is more uniform within the combustion kernel.

Between −5° and + 10°, the SM reveals that the combustion kernel is concentrated around the bowl, justifying the presence of only one peak in the HRR. Conversely, in the cases of SML and TM, two distinct hot areas are clearly visible: one in the bowl and, after several crankshaft angles, another outside the bowl but close to the head of the combustion chamber, attributable to the higher H_2 concentration. Although temperatures are higher in the SML compared to the TM, the difference in maximum temperature between the two hottest areas is smaller in the

SML than in the TM, which explains the second peak in the HRR.

Regarding NOx emissions, Fig. 5(a) shows that TM has low NOx at 500 ppm, compared to the 900 ppm of SML, despite having a higher amount of H_2. In Fig. 15, it can be observed that the maximum temperature in TM is consistently lower than in SML at any crank angle, which can justify the lower level of NOx in TM.

6. Conclusions

This work presents an experimental investigation of the effects of using H_2 as the primary fuel in an ICE. The study explores NOx emissions, efficiency, MEP, SOC, and maximum in-cylinder pressure through experiments, comparing them with WI and CR in a modified high-speed turbocharged common-rail automotive diesel engine. Based on the experimental results, the following conclusions can be drawn from this investigation:

- NOx emissions increase monotonically with CR for any HES, with the rate of increase accelerating as HES and RPM decrease. Within the CR range of 13.5 to 17.5 at 2000 RPM, NOx increases by 80 % at HES 62 %, but at HES 45 %, NOx increases by 400 %.
- NOx emissions increase monotonically with HES for any CR, RPM, or SOI. At 2500 rpm, SOI 10°, CR 17.5, and without WI, going from HES 38 %–55 % (a 45 % increment) results in a 57 % increase in NOx. However, going from HES 55 %–64 % (a 16.3 % increment) leads to a 54 % increase in NOx. This behavior demonstrates the non-linear response of NOx to changes in HES, with the increase in NOx relative to the HES increase being almost cubic.
- Injection of water reduces NOx for the same HES, but NOx tends to be more sensitive to changes in HES than to changes in WI. At 2000 rpm, SOI 10°, and CR 17.5, NOx decreases from 900 ppm to 370 ppm when WI increases from 0 to 0.266 g/cycle. For 77 % HES and CR 16.3, NOx decreases by 41 % with a 100 % increase in WI. Therefore, the effect of WI on NOx reduction becomes less significant as HES increases; as HES increases, the required WI should also increase, following an almost quadratic pattern.
- NOx decreases monotonically with RPM, significantly reducing the range of NOx levels with HES and diminishing the influence of CR and WI on it. For SOI 10° at 2000 rpm, the NOx range is between ~20 and 1000 ppm for all engine loads and WI levels. With the same SOI at 2750 rpm, the NOx levels range from ~20 to 590 ppm. Consequently, an increase in RPM of 37.5 % reduces the maximum NOx by 40 %, resulting in a ratio of $\Delta RPM/\Delta NOx$ of approximately −1 for this SOI.
- SOI has a significant impact on NOx emissions, as even a small reduction in SOI results in a substantial decrease in NOx. For all HES, WI, and CR settings at 2000 rpm with SOI at 10°, the NOx range is between ~20 and 1000 ppm. When the SOI is reduced to 0° at the same RPM, the NOx range narrows to ~20 and 350 ppm. Therefore, a 50 % reduction in SOI leads to a 65 % reduction in NOx, resulting in a $\Delta SOI/\Delta NOx$ ratio of approximately 0.8.
- The combination of different agents, including WI, SOI, CR reduction, and RPM increase, all managed simultaneously, exhibits an accumulative pattern. However, it's important to note that the effects of these different agents cannot be simply added together as if they were acting independently. For example, with an HES of 72 % at SOI 10°, 2000 rpm, CR 17.5, and WI of 0.266 g/cycle, the NOx level is 650 ppm. In contrast, when keeping the same HES but reducing SOI to 5°, increasing RPM to 2750, raising WI to 0.388 g/cycle, and decreasing CR to 14.5, it allows for a reduction in NOx to 100 ppm.
- The parameter α has proven to be highly effective in determining the maximum amount of WI needed to control NOx emissions, ensuring it meets the required limits. As a result, this parameter can be utilized in designing the strategy for NOx control.
- It has been observed that reducing the CR from 17.5:1 to 14.5:1 has a negligible effect on efficiency, remaining nearly constant. It is only when the CR is reduced to 13.5:1 that a decrease in efficiency, approximately 5 %, is observed, which can be attributed to the efficiency cycle penalty. Therefore, it is feasible to maintain high efficiency up to CR 14.5:1 while achieving low NOx levels.
- The operation of the engine using H_2 as the primary fuel is stable and knock-free when combined with WI, up to a MEP of approximately 11.5 bar, the highest value achieved.
- The in-cylinder peak pressure decreased significantly with the reduction in CR. The maximum pressure drop observed was 40 bar between CR 17.5:1 and 13.5:1 for the highest HES.
- WI has several effects regardless of CR: (i) up to a 5 % reduction in efficiency, (ii) a maximum MEP loss of 0.5 bar compared to cases without WI or with a lower amount of water, (iii) a SOC by one or two crank angle degrees, and (iv) a maximum in-cylinder pressure decreases of between 5 and 10 bar.
- It has been demonstrated that it is feasible to transform current diesel engine technology to operate in a stable dual-mode, knock-free manner, where diesel is used solely for ignition. This allows for achieving high efficiency while maintaining minimal NOx levels with WI. These results make it possible to consider H_2 as a viable fuel option for current diesel engine technology, serving as an alternative to fuel cells due to its robustness, cost-effectiveness, high efficiency, and the significant levels of MEP achieved.

Declaration of Competing Interest

The authors declare that they have no known competing financial interests or personal relationships that could have appeared to influence the work reported in this paper.

Data availability

Data will be made available on request.

Acknowledgements

This work was supported by the Junta de Andalucía (Consejería de Economía, Conocimiento, Empresas y Universidad) as part of item PY20 RE 010 within the "Incentivos a los agentes del sistema andaluz del conocimiento – Ayudas a la I + D + i, en el ámbito del Plan Andaluz de Investigación, Desarrollo e Innovación (PAIDI 2020). Authors are also thankful to the Spanish Ministry of Science and Innovation (PID2019-105936RB-C21 and TED2021-130596B-C22).

Annex.

Maximum and minimum values for the H_2 fuel mode studied.

	SOI for pilot injection	H_2 (kg/h)	HES (%)	H_2O (kg/h)	Diesel (kg/h)	Torque (Nm)	Power (kW)	MEP (bar)	Efficiency	Fuel/Air equivalence ratio
CR 17.5:1										

(continued on next page)

(*continued*)

Maximum and minimum values for the H_2 fuel mode studied.

	SOI for pilot injection	H_2 (kg/h)	HES (%)	H_2O (kg/h)	Diesel (kg/h)	Torque (Nm)	Power (kW)	MEP (bar)	Efficiency	Fuel/Air equivalence ratio
1500	10°	0–0.9	0–78	0–48	0.74	2.0–70.2	0.32–10.6	0.17–5.76	0.04–0.28	0.14–0.45
RPM	5°					2–72	0.32–11	0.17–5.89	0.04–0.29	0.15–0.45
	0°					2.6–78.2	0.41–12.4	0.22–6.72	0.05–0.32	0.15–0.41
2000	10°	0–1.5	0–81	0–48	1.08	2.5–98.0	0.53–20.7	0.21–8.42	0.05–0.33	0.14–0.30
RPM	5°	0–1.8	0–83			3.0–120.5	0.64–25.5	0.26–10.36	0.05–0.35	0.16–0.33
	0°	0–2.0	0–85			2.6–131.8	0.55–27.6	0.22–11.3	0.04–0.36	0.15–0.33
2500	10°	0–2.15	0–81	0–48	1.53	2.0–118.1	0.53–31.2	0.17–10.2	0.03–0.35	0.15–0.28
RPM	5°	0–2.0	0–80			4.5–113.7	1.1–29.9	0.39–9.77	0.07–0.35	0.16–0.18
	0°	0–2.0	0–80			2–109.9	0.52–28.8	0.17–9.45	0.03–0.34	0.17–0.26
2750	10°	0–2.0	0–78	0–48	1.74	7.3–100.0	2.11–28.9	0.63–8.59	0.12–0.34	0.16–0.29
RPM	5°	0–1.8	0–76	0–32		7.1–89.0	2.05–25.7	0.61–7.64	0.12–0.32	0.16–0.25
	0°	0–1.8	0–76	0–32		5.2–89.2	1.50–25.7	0.45–7.67	0.07–0.32	0.17–0.24
CR 16.3:1										
1500	10°	0–1.2	0–82	0–48	0.77	2.9–90.8	0.46–14.3	0.25–7.81	0.05–0.31	0.13–0.5
RPM	5°					4.7–98.4	0.76–15.5	0.40–8.46	0.08–0.32	0.15–0.72
	0°					2.8–101.8	0.45–15.6	0.24–8.75	0.05–0.33	0.13–0.49
2000	10°	0–1.5	0–80	0–48	1.10	3.3–100.4	0.70–21.1	0.28–8.63	0.06–0.34	0.12–0.28
RPM	5°	0–1.8	0–83	0–48		1.3–117.3	0.27–24.9	0.11–10.08	0.02–0.35	0.12–0.37
	0°	0–2.0	0–85	0–48		2.7–132.8	0.57–28.5	0.23–11.42	0.05–0.36	0.13–0.27
2500	10°	0–1.8	0–79	0–48	1.40	3.6–104.5	0.95–27.5	0.31–8.98	0.06–0.36	0.13–0.27
RPM	5°	0–2.0	0–81	0–48		2.2–116.3	0.58–30.6	0.19–10.0	0.04–0.37	0.12–0.19
	0°	0–1.8	0–79	0–32		3.5–104.7	0.92–27.43	0.30–9.0	0.05–0.36	0.14–0.19
2750	10°	0–1.8	0–76	0–32	1.74	7.4–96.7	2.13–27.8	0.64–8.31	0.12–0.35	0.13–0.25
RPM	5°	0–1.5	0–72	0–32		10.5–79.4	3.03–22.8	0.90–6.83	0.16–0.32	0.13–0.24
CR 15.5:1										
1500	10°	0–1.2	0–83	0–48	0.76	2.4–92	0.38–14.52	0.21–7.91	0.05–0.31	0.13–0.48
RPM	5°			0–48		3.7–98.3	0.58–15.61	0.32–8.45	0.07–0.32	0.13–0.49
	0°			0–16		3.8–102.2	0.60–16.19	0.33–8.79	0.07–0.33	0.14–0.51
2000	10°	0–1.5	0–81	0–48	1.08	4.5–96.9	0.94–20.4	0.39–8.33	0.08–0.33	0.13–0.41
RPM	5°			0–48		4.5–96.9	0.95–20.4	0.39–8.33	0.09–0.34	0.12–0.36
	0°			0–32		4.2–105.2	0.88–22.21	0.36–9.04	0.07–0.35	0.13–0.31
2500	10°	0–2.15	0–81	0–48	1.54	3.6–120.2	0.94–31.61	0.31–10.33	0.06–0.36	0.12–0.25
RPM	5°	0–2.0	0–80	0–48		3.7–110	0.97–28.82	0.32–9.46	0.06–0.35	0.14–0.23
	0°	0–1.8	0–78	0–32		4.8–96.6	1.26–25.32	0.41–8.30	0.07–0.32	0.15–0.22
2750	10°	0–1.8	0–75	0–48	1.78	4.4–11.1	1.27–25.73	0.38–7.67	0.07–0.32	0.13–0.21
RPM	5°	0–1.8	0–75	0–32		3–85.2	0.87–24.62	0.26–7.32	0.04–0.30	0.14–0.21
	0°	0–1.5	0–72	0–16		4.3–60	1.24–17.30	0.37–5.16	0.05–0.24	0.15–0.19
CR 14.5:1										
1500	10°	0–0.9	0–78	0–32	0.76	0.3 –71.7	0.05–11.31	0.03–6.16	0.01–0.29	0.14–0.39
RPM	5°	0–0.3	0–55	0–16		2.1–27.8	0.33–4.38	0.18–2.39	0.04–0.24	0.14–0.26
	0°	0–0.6	0–70	0		2.1–58.4	0.33–9.18	0.18–5.02	0.04–0.31	0.16–0.29
2000	10°	0–1.5	0–80	0–48	1.13	3.1–102.3	0.65–21.5	0.27–8.79	0.06–0.34	0.15–0.28
RPM	5°	0–1.8	0–83	0–48		3.3–125.9	0.7–26.39	0.29–10.82	0.06–0.36	0.14–0.3
	0°	0–0.3	0–45	0		2.83–8	0.59–1.68	0.24–0.69	0.03–0.05	0.26–0.31
2500	10°	0–2.0	0–79	0–48	1.71	2–111.8	0.52–29.29	0.17–9.61	0.03–0.35	0.15–0.25
RPM	5°	0–2.0	0–79	0–48		2–110.8	0.53–28.98	0.17–9.52	0.03–0.34	0.15–0.25
	0°	0–1.5	0–72	0–32		5–93.8	1.31–24.64	0.43–8.06	0.05–0.31	0.22–0.27
2750	10°	0–1.5	0–70	0–32	1.97	2–71.7	0.58–20.63	0.17–6.16	0.03–0.29	0.16–0.21
RPM	5°	0–1.5	0–70	0–32		2–66.2	0.58–19.08	0.07–5.69	0.03–0.27	0.16–0.21
	0°	0–1.2	0–65	0–16		3–54.1	0.87–15.67	0.26–4.68	0.03–0.22	0.22–0.24
CR 13.5:1										
1500	10°	0–0.6	0–65	0–16	0.96	1–52.6	0.16–8.28	0.09–4.52	0.02–0.27	0.17–0.45
RPM	5°	0–0.3	0–48	0		1.7–26.5	0.27–4.17	0.15–2.28	0.03–0.2	0.18–0.25
2000	10°	0–1.8	0–82	0–48	1.19	1.9–106.9	0.4–22.5	0.16–9.19	0.03–0.32	0.17–0.29
RPM	5°	0–1.2	0–75	0–32		5.3–88.8	1.11–18.6	0.46–7.63	0.06–0.32	0.22–0.3
2500	10°	0–2.0	0–78	0–48	1.71	2.4–107.9	0.63–28.42	0.21–9.28	0.03–0.33	0.17–0.26
RPM	5°			0–48		4.1–108.2	1.08–28.38	0.35–9.3	0.06–0.32	0.18–0.27
2750	10°	0–1.8	0–73	0–48	1.98	2.7–84.9	0.78–24.5	0.23–7.3	0.04–0.3	0.17–0.23
RPM	5°	0–1.5	0–69	0–16		3.5–70.2	1.01–20.23	0.3–6.03	0.04–0.27	0.19–0.23

References

[1] World Energy Council. Global transport scenarios 2050. WEC London. http://www.worldenergy.org/wp-content/uploads/2012/09/wec_transport_scenarios_2050.pdf.

[2] OPEC. World oil outlook; 2013. http://www.opec.org/opec_web/static_files_project/media/downloads/publications/WOO_2013.pdf.

[3] EU CO2 Emission standards for passenger cars and light-commercial vehicles, Policy Update. International Council on Clean Transportation. ⟨http://www.theicc

t. org/sites/default/files/publications/ICCTupdate_EU-95gram_jan2014.pdf); January 2014 [accessed 03.0315].
[4] Approved delegated act in official EU journal https://eur-lex.europa.eu/legal-content/EN/TXT/?uri=CELEX%3A32021R2139&qid=1639037016630.
[5] EU Technical Expert Group on Sustainable Finance (TEG). Briefing on the eu technical expert group's recommendation for the eu taxonomy electricity generation threshold – 7 key points about the EU Taxonomy's 100g emissions threshold) https://ecostandard.org/wp-content/uploads/2021/12/EUTaxonomy_100g_7points.pdf.
[6] P. Tamilselvana, N. Nallusamy, S. Rajkumar, A comprehensive review on performance, combustion and emission characteristics of biodiesel fueled diesel engines, Renew. Sustain. Energy Rev. 79 (2017) 1134–1159.
[7] J.A. Vélez Godiño, M. Torres García, F.J. Jiménez-Espadafor Aguilar, Experimental analysis of late direct injection combustion mode in a compression-ignition engine fuelled with biodiesel/diesel blends, Energy 239 (2022) 121895.
[8] D.H. Qi, K. Yang, D. Zhang, B. Chen, Combustion and emission characteristics of diesel-tung oil-ethanol blended fuels used in a CRDI diesel engine with different injection strategies, Appl. Therm. Eng. 111 (2017) 927–935.
[9] D. Qi, K. Li, C. Zhang, T. Wang, Effect of split injection strategies on diverse characteristics of a common rail direct injection diesel engine operating with diesel-palm oil-ethanol micro-emulsions, Proc. Instit. Mech. Eng. Part a: J. Power Energy 236 (2022).
[10] J. Hwang, D. Qi, Y. Jung, C. Bae, Effect of injection parameters on the combustion and emission characteristics in a common-rail direct injection diesel engine fueled with waste cooking oil biodiesel, Renew. Energy 63 (2014) 9–17.
[11] H.A. Alrazen, A.R. Abu Talib, R. Adnan, K.A. Ahmad, A review of the effect of hydrogen addition on the performance and emissions of the compression – Ignition engine, Renew. Sustain. Energy Rev. 54 (2016) 785–796, https://doi.org/10.1016/j.rser.2015.10.088. ISSN 1364-0321.
[12] M. Gurz, E. Baltacioglu, Y. Hames, K. Kaya, The meeting of hydrogen and automotive: A review, Int. J. Hydrogen Energy 42 (36) (2017) 23334–23346, https://doi.org/10.1016/j.ijhydene.2017.02.124. ISSN 0360-3199.
[13] K. Konstantinos, O. Hertel, M. Ketzel, R. Berkowicz, Operational street pollution model (OSPM) – A review of performed application and validation studies and future prospects, Environ. Chem. 7 (6) (2010) 485–503.
[14] S.E. Hosseini, M.A. Wahid, Hydrogen production from renewable and sustainable energy resources: promising green energy carrier for clean development, Renew. Sustain. Energy Rev. 57 (2016) 850–866.
[15] R. Moradi, K.M. Groth, Hydrogen storage and delivery: Review of the state of the art technologies and risk and reliability analysis, Int. J. Hydrogen Energy 44 (2019) 12254–12269.
[16] S. Zinatloo-Ajabshir, Z. Salehi, O. Amiri, M. Salavati-Niasari, Green synthesis, characterization and investigation of the electrochemical hydrogen storage properties of Dy2Ce2O7 nanostructures with fig extract, Int. J. Hydrogen Energy 44 (36) (2019) 20110–20120.
[17] M. Rezayeenik, M. Mousavi-Kamazani, S. Zinatloo-Ajabshir, CeVO4/rGO nanocomposite: facile hydrothermal synthesis, characterization, and electrochemical hydrogen storage, Appl. Phys. A 129 (2023) 47.
[18] S. Zinatloo-Ajabshir, M.S. Morassaei, O. Amiri, M. Salavati-Niasari, L.K. Foong, Nd2Sn2O7 nanostructures: Green synthesis and characterization using date palm extract, a potential electrochemical hydrogen storage material, Ceram. Int. 46 (2020) 17186–17196.
[19] S. Zinatloo-Ajabshir, Z. Salehi, M. Salavati-Niasari, Synthesis of dysprosium cerate nanostructures using Phoenix dactylifera extract as novel green fuel and investigation of their electrochemical hydrogen storage and Coulombic efficiency, J. Clean. Prod. 215 (2019) 480–487.
[20] S. Verhelst, T. Wallner, Hydrogen-fueled internal combustion engines, Prog. Energy Combust. Sci. 35 (6) (2009) 490–527, https://doi.org/10.1016/j.pecs.2009.08.001. ISSN 0360-1285.
[21] V.S. Yadav, S.L. Soni, D. Sharma, Engine performance of optimized hydrogen-fueled direct injection engine, Energy 65 (2014) 116–122, https://doi.org/10.1016/j.energy.2013.12.007. ISSN 0360-5442.
[22] V. Chintala, K.A. Subramanian, Experimental investigations on effect of different compression ratios on enhancement of maximum hydrogen energy share in a compression ignition engine under dual-fuel mode, Energy 87 (2015) 448–462, https://doi.org/10.1016/j.energy.2015.05.014. ISSN 0360-5442.
[23] M. Kumar, T. Tsujimura, Y. Suzuki, NOx model development and validation with diesel and hydrogen/diesel dual-fuel system on diesel engine, Energy 145 (2018) 496–506, https://doi.org/10.1016/j.energy.2017.12.148. ISSN 0360-5442.
[24] G.A. Karim, Hydrogen as a spark ignition engine fuel, Int. J. Hydrogen Energy 28 (5) (2003) 569–577, https://doi.org/10.1016/S0360-3199(02)00150-7.
[25] A. Mohammadi, M. Shioji, Y. Nakai, W. Ishikura, E. Tabo, Performance and combustion characteristics of a direct injection SI hydrogen engine, Int. J. Hydrogen Energy 32 (2) (2007) 296–304, https://doi.org/10.1016/j.ijhydene.2006.06.005.
[26] S. Szwaja, K. Grab-Rogalinski, Hydrogen combustion in a compression ignition diesel engine, Int. J. Hydrogen Energy 34 (10) (2009) 4413–4421, https://doi.org/10.1016/j.ijhydene.2009.03.020. ISSN 0360-3199.
[27] C. Venkateswarlu, K.A. Subramanian, A comprehensive review on utilization of hydrogen in a compression ignition engine under dual fuel mode, Renew. Sustain. Energy Rev. 70 (2017) 472e91, https://doi.org/10.1016/j.rser.2016.11.247.
[28] Z. Sahin, T. Mustafa, D. Orhan, Experimental investigation of the effects of water adding to the intake air on the engine performance & exhaust emissions in a DI automotive diesel engine, Fuel 115 (2014) 884–8957.
[29] J. Serrano, F.J. Jiménez-Espadafor, A. López, Analysis of the effect of different hydrogen/diesel ratios on the performance and emissions of a modified compression ignition engine under dual-fuel mode with water injection, Hydrogen-Diesel Dual-Fuel Mode, Energy. 172 (2019) 702–711, https://doi.org/10.1016/j.energy.2019.02.027.
[30] M. Masood, S.N. Mehdi, P. Ram Reddy, Experimental investigations on a hydrogen-diesel dual fuel engine at different compression ratios, ASME. J. Eng. Gas Turbines Power 129 (2) (2007) 572–578, https://doi.org/10.1115/1.2227418.
[31] R. Adnan, H.H. Masjuki, T.M.I. Mahlia, Performance and emission analysis of hydrogen fueled compression ignition engine with variable water injection timing, Energy 43 (1) (2012) 416–426, https://doi.org/10.1016/j.energy.2012.03.073. ISSN 0360-5442.
[32] J.H. Zhou, C.S. Cheung, W.Z. Zhao, C.W. Leung, Diesel–hydrogen dual-fuel combustion and its impact on unregulated gaseous emissions and particulate emissions under different engine loads and engine speeds, Energy 94 (2016) 110–123, https://doi.org/10.1016/j.energy.2015.10.105. ISSN 0360-5442.
[33] P. Rosha, A. Dhir, S.K. Mohapatra, Influence of gaseous fuel induction on the various engine characteristics of a dual fuel compression ignition engine: A review, Renew. Sustain. Energy Rev. 82 (2018) 3333–3349.
[34] V. Chintala, K.A. Subramanian, Experimental investigation of hydrogen energy share improvement in a compression ignition engine using water injection and compression ratio reduction, Energ. Conver. Manage. 108 (2016) 106–119, https://doi.org/10.1016/j.enconman.2015.10.069. ISSN 0196-8904.
[35] P. Raju, S. Masimalai, Numerical study on a diesel-hydrogen dual-fuel engine with water injection and variable compression ratio, Energ. Technol. 10 (2022) 2100626, https://doi.org/10.1002/ente.202100626.
[36] V. Chintala, K.A. Subramanian, Hydrogen energy share improvement along with NOx (oxides of nitrogen) emission reduction in a hydrogen dual-fuel compression ignition engine using water injection, Energy Convers Manag. 83 (2014) 249–259, https://doi.org/10.1016/j.enconman.2014.03.075.
[37] V. Chintala, K.A. Subramanian, An effort to enhance hydrogen energy share in a compression ignition engine under dual-fuel mode using low temperature combustion strategies, Appl. Energy 146 (2015) 174–183, https://doi.org/10.1016/J.APENERGY.2015.01.110.
[38] P. Rosha, S. Kumar, P. Senthil Kumar, C.N. Kowthaman, S. Kumar Mohapatra, A. Dhir, Impact of compression ratio on combustion behavior of hydrogen enriched biogas-diesel operated CI engine, Fuel 310 (2022), https://doi.org/10.1016/j.fuel.2021.122321.
[39] I.T. Yilmaz, The effect of hydrogen on the thermal efficiency and combustion process of the low compression ratio CI engine, Appl. Therm. Eng. 197 (2021), https://doi.org/10.1016/j.applthermaleng.2021.117381.
[40] https://www.kistler.com/ES/es/cp/water-cooled-cylinder-pressure-sensors-6041b/P0000393.
[41] http://www.skynam.com/category.php?id_category=18.
[42] S. Bhoite, B. Windom, J. Singh, D. Montgomery, A.J. Marchese, A study of ignition and combustion of liquid hydrocarbon droplets in premixed fuel/air mixtures in a rapid compression machine, Proc. Combust. Inst. 39 (2) (2023) 2533–2542.